pp 2169–2199.
doi:10.1017/aer.2021.54

Towards a new design with generic modeling and adaptive control of a transformable quadrotor

S.H. Derrouaoui, Y. Bouzid and M. Guiatni
derrouaouish@gmail.com
Complex Systems Control and Simulators (CSCS) Laboratory
Ecole Militaire Polytechnique
Bordj el Bahri, Algiers
Algeria

ABSTRACT

Recently, transformable Unmanned Aerial Vehicles (UAVs) have become a subject of great interest in the field of flying systems, due to their maneuverability, agility and morphological capacities. They can be used for specific missions and in more congested spaces. Moreover, this novel class of UAVs is considered as a viable solution for providing flying robots with specific and versatile functionalities. In this paper, we propose (i) a new design of a transformable quadrotor with (ii) generic modeling and (iii) adaptive control strategy. The proposed UAV is able to change its flight configuration by rotating its four arms independently around a central body, thanks to its adaptive geometry. To simplify and lighten the prototype, a simple mechanism with a light mechanical structure is proposed. Since the Center of Gravity (CoG) of the UAV moves according to the desired morphology of the system, a variation of the inertia and the allocation matrix occurs instantly. These dynamics parameters play an important role in the system control and its stability, representing a key difference compared with the classic quadrotor. Thus, a new generic model is developed, taking into account all these variations together with aerodynamic effects. To validate this model and ensure the stability of the designed UAV, an adaptive backstepping control strategy based on the change in the flight configuration is applied. MATLAB simulations are provided to evaluate and illustrate the performance and efficiency of the proposed controller. Finally, some experimental tests are presented.

Keywords: Transformable quadrotor; Adaptive morphology; Generic modeling; Adaptive control strategy

Received 17 December 2020; revised 9 April 2021; accepted 24 May 2021.

NOMENCLATURE

UAVs	unmanned aerial vehicles
CoG	center of gravity
CAD	computer-assisted design
GC	geometric center
PID	proportional integral derivative
DC	direct current
LQR	linear quadratic regulation
MRAC	model reference adaptive control
LQI	linear quadratic integral
TGB	trajectory generator block
ESCs	electronic speed controllers

1.0 INTRODUCTION

The use of UAVs has increased rapidly over the past decade because they have become an important platform for researchers, due to their versatility, efficiency and simplicity of use. They are exploited in various domains, ranging from civilian applications to specific military missions, such as photography, search-and-rescue operations and surveillance[1–3]. However, several challenges must be addressed before integrating UAVs in these tasks, in particular that of crossing narrow spaces, navigating in unknown and crowded places, transporting and seizing objects, while ensuring optimization of the consumed energy[4]. For example, conventional quadrotors have limitations regarding the capacity of their mechanical structure, and their propellers must be in the horizontal plane during flight, making it very difficult to traverse spaces smaller than the body size with a fixed shape. Moreover, they lack the ability to adapt their aerial morphology to different flight conditions, as is generally observed in birds[5]. Another important point, which concerns the transport of objects, where conventional UAVs must be equipped with one or more manipulator arms. This classic design considerably increases the structural complexity of the UAV, limiting it in the case of several objects, reducing the payload, consuming large amounts of energy, and degrading the flight stability by complicating the control strategy[6,7].

All of these challenges led us to focus on the potential of transformable quadrotors. This class of drones is usually reported as unconventional quadrotors[8], transformable multirotors[9], foldable drones[10,11], bio-inspired UAVs[12], drones with extendable arms[13], morphing geometry quadcopters[14], tilt-arm quadrotors[15], quadcopters with a tilting frame[16], deformable drones[17], agile quadrotors[18], multilink aerial robots[19], drones with adaptive morphology[5], drones with changeable geometry[20], tiltable-rotor aerial vehicles[21], convertible drones[22] or modular drones[23]. Nowadays, the vision of researchers towards such drones and their applications has changed radically, they have opened a new interesting research field in the automation and flying robots community[24]. Unlike conventional UAVs, foldable devices show improved flight performance[10,17,25,26] and offer many advantages such as reduced dimensions for navigation in cluttered places[10,15,18], geometric adaptability[8,10,17], high agility and precision[18,27], high endurance and maneuverability[10,15,17,28] and energy optimization in flight[10,29].

https://doi.org/10.1017/aer.2021.54 Published online by Cambridge University Press

Transformable UAVs enable the performance of various missions, such as flight and navigation in dangerous and difficult-to-access environments, crossing narrow spaces, discovery and inspection of abandoned areas as well as the surveillance of sensitive locations[4,5,30]. They can also be exploited to transport multiple objects of different sizes without additional mechanisms, unlike classic devices[31,32]. In addition, the change of configuration allows the introduction of different movements (roll, pitch and yaw) with rotating and extendable arms but without affecting the rotation speeds of the rotors, enabling an interesting transition from an under- to over-actuated system[33].

1.1 Related works

Many prototypes of transformable multirotors have been proposed in literature by introducing adaptive mechanisms to the conventional structures of multirotors. These mechanisms can act on the orientation of the propellers or rotors, the length or number of arms, the rotation of the arms, etc.

The transition from one configuration to another can be achieved either sequentially, by keeping a fixed altitude, transforming and then continuing the mission, or simultaneously, during the execution of the mission.

The idea proposed in Ref.[15] concerns the design of a novel foldable morphing quadrotor, where the links between the drone arms and the main body are replaced by sprung hinges. According to the authors, this idea allows for the arms to fold downward in the case of weak thrusts produced by the four propellers. This particular quadcopter is designed to execute certain critical missions that a conventional UAV cannot do.

A new design of a miniature quadrotor manufactured using foldable robotics methods for collision resilience was proposed in Ref.[27]. In Ref.[17], a quadrotor based on foldable scissor-shaped structures was developed. The designed structure is based on an angulated element to form a variable curvature. In addition, it allows easy adjustment of the volume of the UAV to adapt it to different obstacles.

In the work presented in Ref.[28], a self-folding quadrotor was presented, where the rotation of the four arms occurs horizontally at the same time using a single servomotor. In Ref.[18], Riviere et al. proposed a quadrotor that can fold its structure through a vertical or tilted window. However, a loss of roll control is observed due to the alignment of the four rotors when the robot is in its folded state.

Xiong et al.[29] dealt with the problem of optimizing the consumed energy of a new quadrotor with rotating arms. The same principle is adopted in Ref.[10] with the purpose of minimizing the energy according to the task to be executed. Another example of a quadrotor with foldable arms was studied by Mintchev et al. in Ref.[34], where the fabrication of this robot is based on an origami technique using multi-layer material. A new design for foldable UAVs was considered in Refs.[25,35], where the angle between the arms can be changed while flying. The disadvantage of these structures is that they are light. However, the payload is not large enough, and the rotation of the four arms is not independent.

Contrary to fixed-wing UAVs, folding-wing devices have the particularity of tilting the wings, as found in birds, thus allowing them to reduce their size[36–38]. Therefore, this tilting process generates less friction drag, which increases the speed of the drone and can maintain a constant ground speed in relatively stronger headwinds[39]. However, this type of UAVs generally presents a difficulty of control, in particular in the presence of wind. There are also consequences in terms of cost, weight and structural complexity.

https://doi.org/10.1017/aer.2021.54 Published online by Cambridge University Press

In Ref.[40], Daler et al. developed a multi-modal folding-wing drone that can switch from aerial mode to a terrestrial morphology by folding its wings under different flight conditions. In addition, its folded wings improve the efficiency of the robot on the ground, while its extended wings maximize lift during flight. The same idea was adopted by Morton et al.[41]. This flying robot can fly as a conventional quadrotor, and when it crosses a narrow place, it folds up and adopts the configuration of a mobile unicycle robot. The disadvantage of this structure is that it cannot pass through a narrow place, only when the robot is located on the plane. A transformable solar UAV[42] with four wing sections has also been realised to improve the performance of solar-powered fixed-wing drones as well as their transformation during flight operation.

Multi-link multirotors are another type of transformable quadrotors. They are equipped with several servomotors and rotors, enabling the aerial robot to switch in flight to accomplish the desired tasks.

A transformable multirotor UAV composed of multiple two-dimensional links was developed by Zhao et al.[9,43]. This robot is designed to manipulate objects by grabbing them, picking them up, transporting them and dropping them at different places. The limitation of this structure is that it cannot transform during movement, i.e., it must be maintained at a fixed altitude to fold up. Zhao et al.[19] proposed another multi-link multirotor. This structure is inspired by the ability of a snake to traverse a small hole by changing its shape. However, the large number of rotors and servomotors makes the folding process very difficult, complex and slow. The design proposed in Ref.[44] is for a reconfigurable multi-linked micro aerial vehicle, capable of transporting objects, crossing narrow places and finding the best way to avoid collision with obstacles.

Bio-inspired transformable UAVs have become one of the most widely used systems among recent aeronautical technologies[45]. In addition, due to the limits on the morphology of classical quadrotors, some researchers[12,46–49] have been inspired by the capacities seen in birds and insects, to make drones that are capable of navigating in congested and narrow places and folding or deforming in the event of a collision with different obstacles to avoid damages. This new solution has become crucial recently, because it has overcome several problems encountered previously in UAVs, namely geometric adaptation.

UAVs with extendable arms offer the possibility of reducing the dimensions of multirotors, where the horizontal surface of the quadrotor is preserved. The arm length reduction is usually achieved using servomotors and a gear system.

Transformable quadrotors that can extend and rotate their arms were proposed in Ref.[13]. The introduced mechanisms make such UAVs over-actuated systems. Therefore, the designed structures are assumed to be symmetrical to facilitate their study. Another transformable quadrotor was considered by Kamil et al. in Ref.[50]. Their design is mainly based on a variation of the length of the four arms to obtain a yaw movement, without modifying the speeds of the rotors, contrary to the conventional quadrotor.

A new design for a morphing quadrotor was presented in Ref.[26], where the authors considered the extension and rotation of the quadrotor arms, which are nevertheless held fixed in the event of a rotor failure to ensure stable flight with three rotors. Only the design and modeling were treated in this work. Due to the unshielded propellers of delivery drones, a novel UAV that can extend and retract its four arms was fabricated and described in Ref.[14].

Tilt-rotor UAVs have been proposed in different research works[21,51–56], and tilt-body UAVs were presented in Refs[16,57,58], are another category of transformable UAVs that presents several advantages such as enhanced agility and precision, high endurance and maneuverability, adjustment of the thrust force by compensation in the event of a breakdown, horizontal and

https://doi.org/10.1017/aer.2021.54 Published online by Cambridge University Press

vertical displacement, elimination of the over-actuation problem and higher speed. However, the main disadvantage of tilting rotors is their poor hover performance caused by the small rotor diameters and large rotor mast. In addition, hovering may not be stable at a large inclination of the rotors because the lift forces are affected by this inclination.

Modular UAVs such as those proposed in Refs[23,59–61] are a new class of transformable UAVs, being composed of different modules that are interconnected with each other. This modularity allows such UAVs to become more flexible, encouraging their use in the areas of transport, parachuting and search and rescue.

Synthesizing these different proposed designs, it can be concluded that most of these structures are complex and have slow transformation mechanisms and high cost. The main goal of the current design is to improve these prototypes and the performance of the mechanical structure of our transformable quadrotor.

1.2 Contributions

This paper is an extension of our previous work[33] in which we only dealt with the problem of modeling this new type of UAVs. However, in this article, as a first contribution, we propose a new design for a transformable quadrotor, where simple and light mechanical mechanisms are introduced. Moreover, as a second contribution, we propose a detailed generic model, which takes into account aerodynamic and gyroscopic effects, the variation of the Centre of Gravity (CoG), the variation of the inertia as well as the variation of the allocation matrix. The final contribution of this paper concerns the proposition of an adaptive control strategy, which has not been previously exploited in transformable quadrotors. This strategy adapts to all of these variations when the quadrotor changes its geometry while flying.

1.3 Outline

The rest of this paper is organised as follows: In Section 2, we present the mechanical design, geometric description and study of the variation of the CoG and inertia. Section 3 explains the different steps followed to obtain the detailed generic model. The design and architecture of the proposed controller are detailed in Section 4. Simulation results are shown in Section 5. A primary prototype of the realised quadrotor, with some experiments, are presented in Section 6. Conclusions and future work are described in Section 7.

2.0 MECHANICAL DESIGN

This section provides a detailed view of the new mechanical design of the transformable quadrotor that we manufactured in our laboratory, as well as the inertia and CoG analyses.

2.1 General description of the transformable quadrotor

The designed quadrotor has four rotating arms as shown in Figs 1, 2 and 3. To achieve a reconfigurable geometry, these arms must be rotated independently, respecting the angle of rotation $\psi_i(t)|_{i=1,\dots,4}$. The angle between each propeller in its horizontal state (parallel to y_m-axis) and its corresponding arm (in the vertical state) is 28.70°. In addition, for improved security and to avoid collisions of the propellers, we slightly shifted two rotors vertically so that the propellers never overlap. We emphasize that the rotation mechanism is simple, using a low-cost frame and having lower weight.

The position of the CoG moves when the quadrotor configuration changes. Consequently, the inertia matrix and roll and pitch moments in this case vary depend on the orientations of

https://doi.org/10.1017/aer.2021.54 Published online by Cambridge University Press

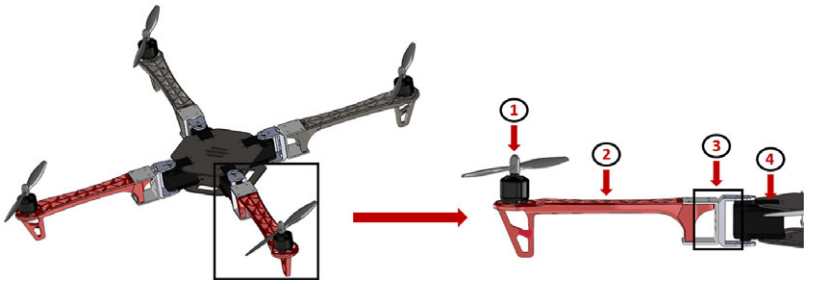

Figure 1. Design of the transformable quadrotor that can change its configuration while flying. Each rotor is connected to a rotating arm. Each rotating arm is actuated by a servomotor and can rotate independently. Each servomotor is linked to a central body. (1) Propeller. (2) Rotating arm. (3) Servo-arm junction. (4) Servomotor.

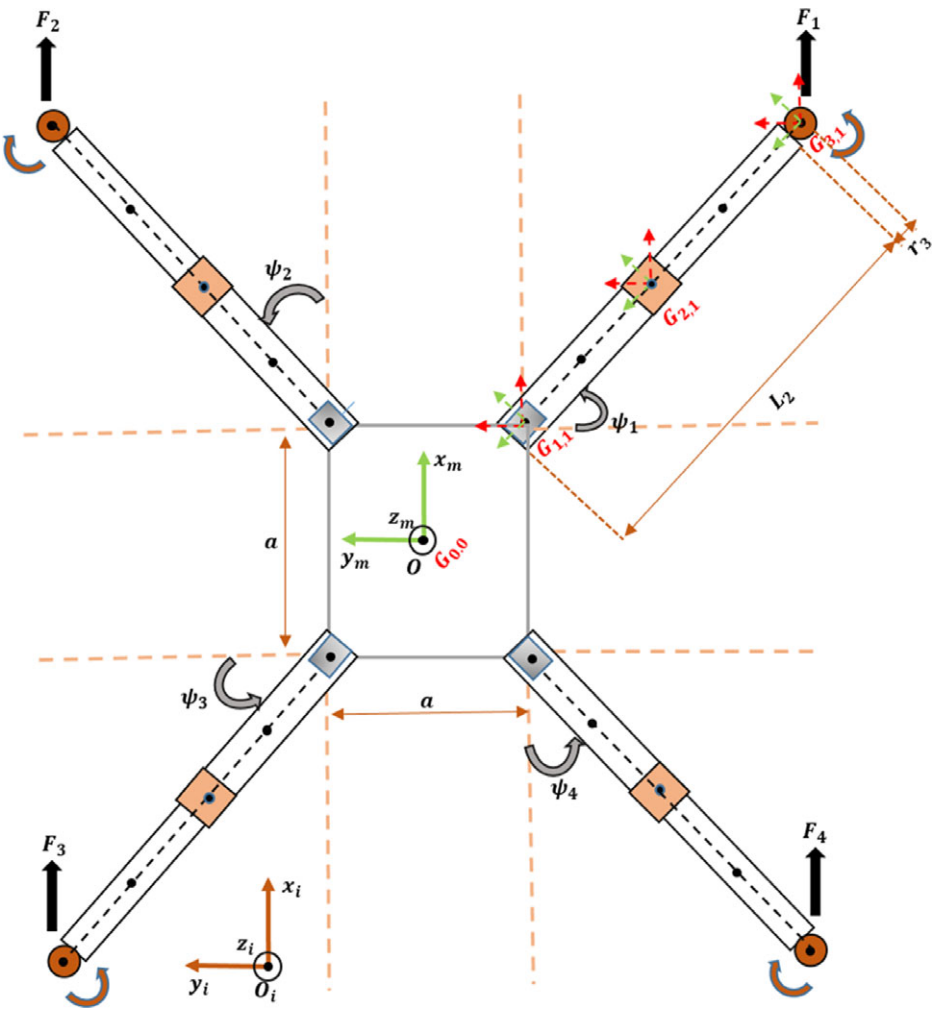

Figure 2. Schematic of the designed transformable quadrotor.

https://doi.org/10.1017/aer.2021.54 Published online by Cambridge University Press

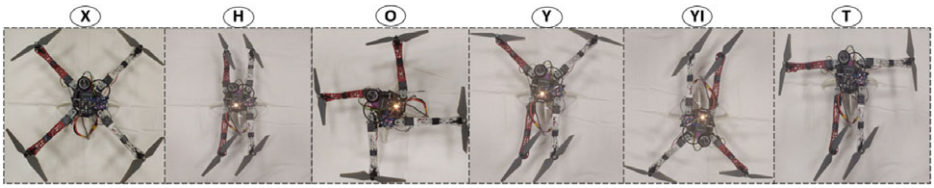

Figure 3. Designed configurations.

Table 1
Characteristics of the configurations

Configurations	Arm angles
X	$\psi_1(t)=\pi/4$, $\psi_2(t)=\pi/4$, $\psi_3(t)=\pi/4$, $\psi_4(t)=\pi/4$
H	$\psi_1(t)=\pi/2$, $\psi_2(t)=0$, $\psi_3(t)=\pi/2$, $\psi_4(t)=0$
O	$\psi_1(t)=\pi$, $\psi_2(t)=\pi$, $\psi_3(t)=\pi$, $\psi_4(t)=\pi$
Y	$\psi_1(t)=\pi/4$, $\psi_2(t)=\pi/4$, $\psi_3(t)=\pi/2$, $\psi_4(t)=0$
YI	$\psi_1(t)=\pi/2$, $\psi_2(t)=0$, $\psi_3(t)=\pi/4$, $\psi_4(t)=\pi/4$
T	$\psi_1(t)=0$, $\psi_2(t)=\pi/2$, $\psi_3(t)=\pi/2$, $\psi_4(t)=0$

the arms. They are written respectively as $\mathfrak{I}_{3\times3}(\psi_i(t))$, $\tau_\varphi(\psi_i(t))$ and $\tau_\theta(\psi_i(t))$. The total thrust $\mathcal{T}$ and the moment around the z_m-axis do not depend on the configuration, and their expressions are the same as those for the classical quadrotor. The central body and servomotors do not rotate around the z_m-axis, whilst the arms and rotors rotate around the same axis. The main configuration leads to many other possible configurations by rotating the arms. Moreover, by changing the speed of the four rotors $\Omega_i|_{i=1,\dots,4}$ or the position of the arms, the quadrotor can produce different motions (roll, pitch, yaw and translation).

The designed quadrotor is considered to be a body assembly composed of a central body of mass $\mathfrak{m}_0$, four servomotors attached to the central body of mass $\mathfrak{m}_{1,i}$, four rotating arms attached to servomotors of mass $\mathfrak{m}_{2,i}$ and four rotors of mass $\mathfrak{m}_{3,i}$. The four rotors are numbered 1, 2, 3 and 4, and each arm is numbered according to the rotor fixed on it. We stress that the axes of rotation of the rotors and rotating arms are parallel to the z_m-axis (Fig. 2).

By actuating the rotation servomotors, the designed quadrotor can transform during flight from the well-known "X" configuration to other particular configurations depending on the flight environment and designated tasks. Each configuration is defined by the angles of rotation of the quadrotor arms $\psi_i(t)$. Figure 3 and Table 1 show the six morphologies that we have used. The choice of these latter is based mainly on their advantages and complexity.

2.2 Inertia and centre of gravity analysis

Since the majority of the considered morphologies are asymmetrical, and to validate the calculations for their use in the generic model and simulation (Sections 3 and 5), the inertia and the global CoG position are determined by two different methods:

2.2.1 Computer-Assisted Design (CAD)-based calculation

Three-Dimensional (3D) CAD modeling of the UAV using SolidWorks software (Figs 1 and 3) allows the direct calculation of the inertias $\mathfrak{I}_{xx}$, $\mathfrak{I}_{yy}$, $\mathfrak{I}_{zz}$, $\mathfrak{I}_{xy}=\mathfrak{I}_{yx}$ and CoG of each

https://doi.org/10.1017/aer.2021.54 Published online by Cambridge University Press

Table 2
CoG coordinates of the considered configurations

	$x(m)$	$y(m)$	$z(m)$
X	0	0	0.00988269
H	0	0	0.00988269
O	0	0	0.00988269
Y	−0.01231197	0	0.00988269
YI	0.01231198	0	0.00988269
T	−0.04203570	0	0.00988269

Table 3
Inertias of the considered configurations

	$\mathfrak{I}_{xx}$ (kg m^2)	$\mathfrak{I}_{yy}$ (kg m^2)	$\mathfrak{I}_{zz}$ (kg m^2)	$\mathfrak{I}_{xy}$ (kg m^2)
X	1.211×10^{-2}	1.213×10^{-2}	2.370×10^{-2}	0
H	2.888×10^{-3}	1.978×10^{-2}	2.112×10^{-2}	-4.1×10^{-10}
O	4.719×10^{-3}	7.743×10^{-3}	7.491×10^{-3}	0
Y	7.10^{-3}	1.596×10^{-2}	2.241×10^{-2}	3×10^{-6}
YI	7×10^{-3}	1.596×10^{-2}	2.241×10^{-2}	-3×10^{-6}
T	1.082×10^{-2}	1.084×10^{-2}	2.112×10^{-2}	0

configuration separately. This will be exploited in this work as a tool to confirm, validate and compare our results with those obtained by the mathematical-based development.

The variation of the CoG coordinates for each configuration calculated in the SolidWorks design environment is presented in Table 2.

We also get the variation of the inertia, as illustrated in Table 3.

2.2.2 Mathematical-based development

The calculation of the inertia and the CoG is based on Assumption 1.

Assumption 1: Each CoG of each subsystem has a green color body frame (Fig. 2), which is assumed to be in the plane (O, x_m, y_m).

2.3 Center of gravity

Unlike a standard quadrotor, the morphology of the proposed UAV is asymmetrical in most cases. Consequently, the CoG varies and must be instantly recalculated and injected into the dynamic model when the configuration is modified. The dynamic formula that estimates the change in the CoG can be represented as follows:

$$\overrightarrow{O\mathbb{G}} = \frac{\sum_{i=1}^{4}\sum_{j=1}^{3} \mathfrak{m}_{j,i}\overrightarrow{O\mathbb{G}_{j,i}}}{\mathfrak{m}_0 + \sum_{i=1}^{4}\sum_{j=1}^{3} \mathfrak{m}_{j,i}} \quad \ldots (1)$$

https://doi.org/10.1017/aer.2021.54 Published online by Cambridge University Press

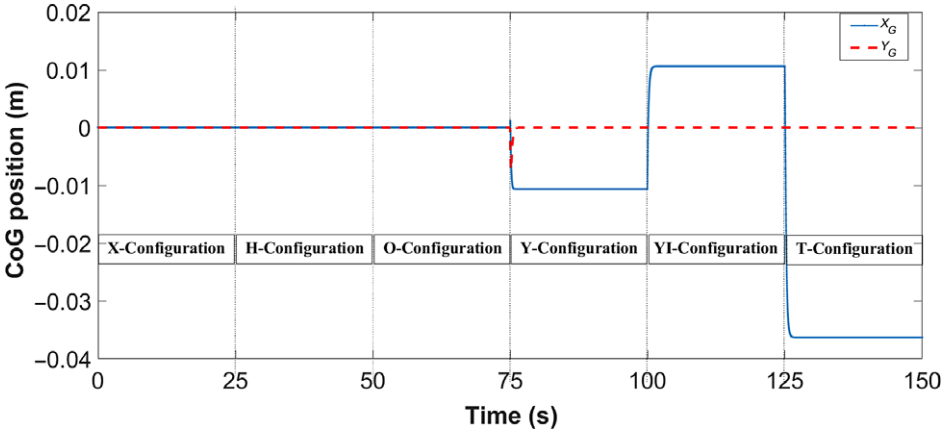

Figure 4. Evolution of the CoG for the different configurations.

with

$$\overrightarrow{O\mathbb{G}} = \begin{bmatrix} x_G \\ y_G \\ z_G \end{bmatrix}, \overrightarrow{O\mathbb{G}_0} = \begin{bmatrix} x_0 \\ y_0 \\ z_0 \end{bmatrix}, \overrightarrow{O\mathbb{G}_{1,i}} = \begin{bmatrix} x_{1,i} \\ y_{1,i} \\ z_{1,i} \end{bmatrix} \quad \ldots (2)$$

$$\overrightarrow{O\mathbb{G}_{2,i}} = \begin{bmatrix} x_{2,i} \\ y_{2,i} \\ z_{2,i} \end{bmatrix}, \overrightarrow{O\mathbb{G}_{3,i}} = \begin{bmatrix} x_{3,i} \\ y_{3,i} \\ z_{3,i} \end{bmatrix} \quad \ldots (3)$$

O : the geometric centre (the origin of the body frame).
$\overrightarrow{O\mathbb{G}} \in \mathbb{R}^{3\times1}$: the offset between the geometric centre of the system and the global CoG.
$\overrightarrow{O\mathbb{G}_0} \in \mathbb{R}^{3\times1}$: the CoG coordinates of the central body.
$\overrightarrow{O\mathbb{G}_{1,i}} \in \mathbb{R}^{3\times1}$: the CoG coordinates of the servomotors.
$\overrightarrow{O\mathbb{G}_{2,i}} \in \mathbb{R}^{3\times1}$: the CoG coordinates of the rotating arms.
$\overrightarrow{O\mathbb{G}_{3,i}} \in \mathbb{R}^{3\times1}$: the CoG coordinates of the rotors.

The evolution of the CoG position for each flight configuration, obtained using approximate calculation functions in MATLAB software, is shown in Fig. 4. In fact, the calculation formula given by Equation (1) takes into account all the intermediate cases; i.e. the transition from one configuration to another is included in the calculation.

2.4 Inertia matrix

The calculation of the inertia for a compound system and elements with a non-regular form is not obvious. Therefore, some approximations should be made to simplify the mathematical development.

The equations that model the variation of the inertia matrix will be developed for each part and finally for the complete system. Using the Huygens–Steiner theorem, the variable inertia matrices are calculated as

https://doi.org/10.1017/aer.2021.54 Published online by Cambridge University Press

$$I_{(0)/O} = m_0 diag\left(\frac{a^2+h_0^2}{12}, \frac{a^2+h_0^2}{12}, \frac{2a^2}{12}\right)_{\mathbb{G}_0} \quad \ldots(4)$$

where $I_{(0)/O}$ is the inertia matrix of the central body, a represents its length and width together and h_0 its height.

The servomotors are assumed to be rectangular cuboids with length of L_1, width of w_1 and height of h_1. Their inertia matrices are given as follows:

$$I_{(1,i)/O} = I_{\mathbb{G}_{1,i}} + m_{(1,i)} \begin{bmatrix} y_{1,i}^2 & -x_{1,i}y_{1,i} & 0 \\ -x_{1,i}y_{1,i} & x_{1,i}^2 & 0 \\ 0 & 0 & x_{1,i}^2 + y_{1,i}^2 \end{bmatrix} \quad \ldots(5)$$

where

$$I_{\mathbb{G}_{1,i}} = m_{(1,i)} diag\left(\frac{L_1^2+h_1^2}{12}, \frac{w_1^2+h_1^2}{12}, \frac{L_1^2+w_1^2}{12}\right)_{\mathbb{G}_{1,i}} \quad \ldots(6)$$

The rotating arms are also supposed to be rectangular cuboid with length of L_2, width of w_2 and height of h_2. Their inertia matrices are determined by the following formula:

$$I_{(2,i)/O_{(Rot)}} = R_z(\psi_i(t)) I_{(2,i)/O} R_z(\psi_i(t))^T \quad \ldots(7)$$

where

$$I_{(2,i)/O} = I_{\mathbb{G}_{2,i}} + m_{(2,i)} \begin{bmatrix} y_{2,i}^2 & -x_{2,i}y_{2,i} & 0 \\ -x_{2,i}y_{2,i} & x_{2,i}^2 & 0 \\ 0 & 0 & x_{2,i}^2 + y_{2,i}^2 \end{bmatrix} \quad \ldots(8)$$

$$I_{\mathbb{G}_{2,i}} = m_{(2,i)} diag\left(\frac{{L_2}^2+h_2^2}{12}, \frac{w_2^2+h_2^2}{12}, \frac{{L_2}^2+w_2^2}{12}\right)_{\mathbb{G}_{2,i}} \quad \ldots(9)$$

and $R_z(\psi_i(t)) \in \mathbb{R}^{3\times3}$ is the rotation matrix on the z_b axis.

The rotors are assumed to be cylinders with radius of r_3 and height of h_3. Their inertia matrices are expressed as

$$I_{(3,i)/O_{(Rot)}} = R_z(\psi_i(t)) I_{(3,i)/O} R_z(\psi_i(t))^T \quad \ldots(10)$$

where

$$I_{(3,i)/O} = I_{\mathbb{G}_{3,i}} + m_{(3,i)} \begin{bmatrix} y_{3,i}^2 & -x_{3,i}y_{3,i} & 0 \\ -x_{3,i}y_{3,i} & x_{3,i}^2 & 0 \\ 0 & 0 & x_{3,i}^2 + y_{3,i}^2 \end{bmatrix} \quad \ldots(11)$$

$$I_{\mathbb{G}_{3,i}} = m_{(3,i)} diag\left(\frac{{r_3}^2}{4} + \frac{h_3^2}{12}, \frac{{r_3}^2}{4} + \frac{h_3^2}{12}, \frac{{r_3}^2}{2}\right)_{\mathbb{G}_{3,i}} \quad \ldots(12)$$

Finally, we obtain the global inertia matrix of the system, which depends on the angle of rotation of each arm $\psi_i(t)$, as

$$\Im_{3\times3}(\psi_i(t)) = I_{(0)/O} + \sum_{i=1}^{4} I_{(1,i)/O} + \sum_{i=1}^{4} I_{(2,i)/O_{(Rot)}} + \sum_{i=1}^{4} I_{(3,i)/O_{(Rot)}} \quad \ldots(13)$$

The evolution of the inertia for the six aerial configurations is shown in Fig. 5.

https://doi.org/10.1017/aer.2021.54 Published online by Cambridge University Press

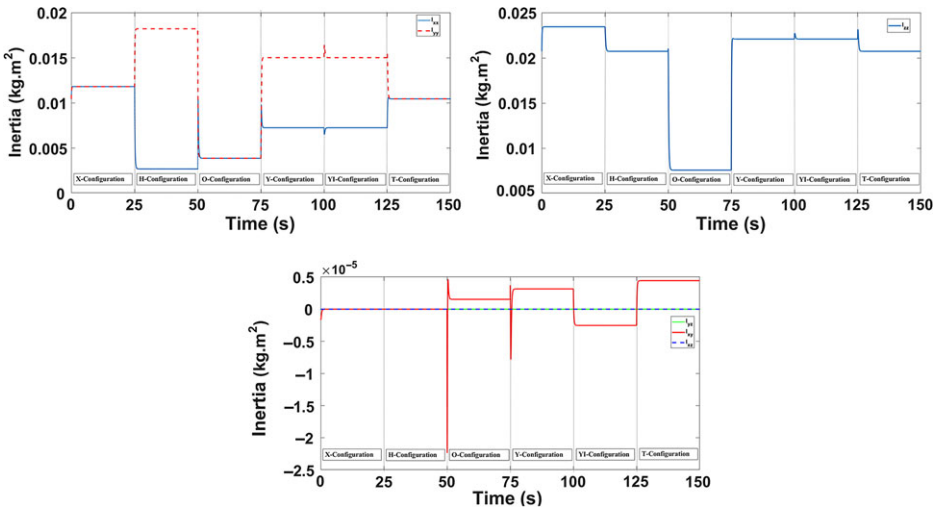

Figure 5. Evolution of inertia along the x_m, y_m and z_m axes as well as the inertia of the non-diagonal terms.

Table 4
Inertia errors

Error	e_{xx}	e_{yy}	e_{zz}	e_{xy}
Error value (kg m^2)	10^{-4}	10^{-4}	10^{-4}	10^{-5}

2.5 Results and discussion

On the basis of the results obtained by SolidWorks CAD (Table 3) and the inertias calculated by the approximate formulas (Fig. 5), the errors between the two methods according to the different axes are summarised in Table 4:

The small difference between the values given by the two methods as shown in Table 4 is justified by the assumptions imposed on the geometry of the quadrotor components.

According to Figs 3 and 4 and Table 2, we can see that, for the configurations "X" and "H", the estimated CoG of the system is confused with the CoG given by SolidWorks, where its values $x(m)$ and $y(m)$ are equal to zero. We can explain this by the symmetry of the configurations along the two axes x_m and y_m. In fact, the "O" configuration is not geometrically symmetrical about the x_m and y_m axes, but it is symmetrical in terms of the mass distribution in relation to these axes. For the "Y", "YI" and "T" configurations, the ordinates $y(m)$ of the CoG are equal to zero. This is justified by the symmetry of these configurations with respect to the x_m-axis. However, the abscissas $x(m)$ are different from zero due to the asymmetry with respect to the y_m-axis, where the error in this case is on the order of 10^{-3}(m).

3.0 GENERIC MODELING

The development of mathematical models for transformable quadrotors has recently become an important aim for many researchers. However, in the literature there is no generic and precise model for this particular class of quadrotors, which is more challenging due

https://doi.org/10.1017/aer.2021.54 Published online by Cambridge University Press

to the variation and complexity of the mechanical structure. Some authors have developed a dynamic model for a quadrotor with two independent arms[25,35]. To simplify the dynamic model, others considered that the CoG of the transformable drone coincides with the geometric centre[15,26,43] or that its structure is symmetrical[13,28,29,62].

The variation of the flight configuration according to the trajectory and the assigned tasks has a significant effect on the position of the CoG of the quadrotor as well as its inertia and allocation matrix. In addition, to establish the mathematical model, we will use the formula that calculates the displacement of the CoG, the equations which model the variation of the inertia matrix and finally the dynamic allocation matrix.

The main objective of this section is to develop a detailed generic model that takes into account all these variations as well as all aerodynamic and gyroscopic effects.

3.1 Flight dynamics

The flight dynamics of the aerial vehicle is described in two coordinate frames, as shown previously in Fig. 2. The inertial frame $\mathfrak{R}_i(O_i, x_i, y_i, z_i)$ is assumed to be fixed while $\mathfrak{R}_m(O, x_m, y_m, z_m)$ is considered to be a mobile frame. Unlike most conventional quadrotors, the CoG does not coincide with the Geometric Center (GC).

Assumption 2: The central body of the quadrotor, servomotors, rotation arms and propellers are assumed to be rigid and totally symmetrical with respect to their own frames.

The rotation from the mobile reference system $\mathfrak{R}_m$ to the inertial fixed frame $\mathfrak{R}_i$ is achieved by three successive rotations around $X-Y-Z$ axes, meaning that the attitude is obtained first by the roll angle φ, then by the pitch angle θ and then by the yaw angle ψ.

The direction cosine matrix, denoted R[63], from the mobile frame $\mathfrak{R}_m$ to the inertial fixed frame $\mathfrak{R}_i$ can be expressed as

$$\mathrm{R}=\begin{bmatrix} \mathrm{c}_\psi \mathrm{c}_\theta & \mathrm{c}_\psi \mathrm{s}_\theta \mathrm{s}_\varphi - \mathrm{s}_\psi \mathrm{c}_\varphi & \mathrm{c}_\psi \mathrm{s}_\theta \mathrm{c}_\varphi + \mathrm{s}_\psi \mathrm{s}_\varphi \\ \mathrm{s}_\psi \mathrm{c}_\theta & \mathrm{s}_\psi \mathrm{s}_\theta \mathrm{s}_\varphi + \mathrm{c}_\psi \mathrm{c}_\varphi & \mathrm{s}_\psi \mathrm{s}_\theta \mathrm{c}_\varphi - \mathrm{c}_\psi \mathrm{s}_\varphi \\ -\mathrm{s}_\theta & \mathrm{c}_\theta \mathrm{s}_\varphi & \mathrm{c}_\theta \mathrm{c}_\varphi \end{bmatrix} \quad \ldots(14)$$

where $\mathrm{R} \in SO(3) = \{\mathrm{R} \in \mathrm{R}^{3\times 3} | \mathrm{R}^T\mathrm{R} = I_{3\times 3},\ det(\mathrm{R}) = 1\}$ and $s_{(\cdot)}$ and $c_{(\cdot)}$ are abbreviations for $\sin(\cdot)$ and $\cos(\cdot)$, respectively.

The linear and angular velocity vectors of the body in the mobile frame are represented respectively as $\Lambda^m = (u, v, w)^T \in \mathbb{R}^3$ and $\varsigma = (p, q, r) \in \mathbb{R}^3$.

The transformable quadrotor has a mass $\mathfrak{m}$ and a variable inertia $\mathfrak{I}(\psi_i(t)) \in \mathbb{R}^{3\times 3}$, which is calculated with respect to the mobile frame $\mathfrak{R}_m(o_m, x_m, y_m, z_m)$ and depends on the angular positions of the four arms $\psi_i(t)$, where $i = 1, 2, 3, 4$.

Let $\Upsilon = (\varphi, \theta, \psi)^T \in \mathbb{R}^3$ describes the orientation of the mobile and $\xi = (x, y, z)^T \in \mathbb{R}^3$ denotes its position with respect to $\mathfrak{R}_i$.

The relation between the velocities and the external forces $f^m = (f_x^m, f_y^m, f_z^m)^T \in \mathbb{R}^3$ and moments $\tau^m = (\tau_x^m, \tau_y^m, \tau_z^m)^T \in \mathbb{R}^3$, applied to the CoG, can be written using the Newton–Euler formalism as

https://doi.org/10.1017/aer.2021.54 Published online by Cambridge University Press

$$\begin{bmatrix} \mathfrak{m}\mathfrak{I}_{3\times3}(\psi_i(t)) & O_{3\times3} \\ O_{3\times3} & \mathfrak{I}(\psi_i(t)) \end{bmatrix} \begin{bmatrix} \dot{\Lambda}^m \\ \dot{\varsigma} \end{bmatrix} + \begin{bmatrix} \varsigma \times \mathfrak{m}\Lambda^m \\ \varsigma \times \mathfrak{I}(\psi_i(t))\varsigma \end{bmatrix} = \begin{bmatrix} f^m \\ \tau^m \end{bmatrix} \quad \ldots(15)$$

The symbol $O_{3\times3}$ means a 3×3-dimensional zero matrix, and $\times$ denotes the cross product.

3.2 Forces and moments applied to the quadrotor

3.2.1 Forces

The quadrotor is affected by several forces, such as gravity, thrust, hub and drag.

Remark 1: All the parameters used in this subsection are mentioned in Table 5.

The gravity vector $\mathcal{G}=(0, 0, -\mathfrak{m}\mathfrak{g})^T \in \mathbb{R}^3$ is applied along the z_i-axis, where $\mathfrak{g}$ represents the gravity.

The rotation of the four rotors can easily generate a thrust force along the z_{ri}-axis and a hub force in the hub plane (x_{ri}, y_{ri}). Thus, the total thrust force $\mathcal{T}$ is the sum of the forces produced by the rotation of each propeller, expressed in the body frame. In addition, the hub force is defined by two components $\mathcal{U}_{xi}$ and $\mathcal{U}_{yi}$ along two axes x_{ri} and y_{ri} in the plane corresponding to each rotor $\mathfrak{R}_{ri}(o_{ri}, x_{ri}, y_{ri}, z_{ri})$[64]. The $\mathcal{T}, \mathcal{U}_{xi}$ and $\mathcal{U}_{yi}$ forces are expressed as

$$\mathcal{T} = \sum_{i=1}^{4} f_i,\ \mathcal{U}_x = -\sum_{i=1}^{4} \mathcal{U}_{xi},\ \mathcal{U}_y = -\sum_{i=1}^{4} \mathcal{U}_{yi} \quad \ldots(16)$$

where $f_i = C_f \rho A(\Omega_i R_r)^2$ and $\mathcal{U}_i = C_{\mathcal{U}} \rho A(\Omega_i R_r)^2$.

The quadrotor can also produce a drag force (friction force) $\mathcal{D} \in \mathbb{R}^3$ expressed in $\mathfrak{R}_i(o_i, x_i, y_i, z_i)$. This force is due to the movement of the quadrotor body affected by the wind, and can be defined as

$$\begin{aligned} \mathcal{D} &= (\mathcal{D}x\ \mathcal{D}y\ \ \mathcal{D}z)^T \\ &= \text{diag}\left(-\mathcal{K}_{\mathcal{D}x}\ -\mathcal{K}_{\mathcal{D}y}\ -\mathcal{K}_{\mathcal{D}z}\right)\dot{\xi} \end{aligned} \quad \ldots(17)$$

Table 5
Modeling parameters

Parameter	Description
A	Propeller disk area
R_r	Propeller radius
ρ	Air density
$C_{(f,\mathcal{U},\mathcal{L},\mathcal{Q})}$	Aerodynamic coefficients
$\mathfrak{J}_r$	Rotor inertia
Ω	Rotor speed
$\mathcal{K}_{\mathcal{A}(x,y,z)}$	Aerodynamic friction coefficients
$\mathcal{K}_{\mathcal{D}(x,y,z)}$	Translation drag coefficients
$\mathfrak{m}$	Quadrotor mass
$\mathfrak{g}$	Gravity coefficient

https://doi.org/10.1017/aer.2021.54 Published online by Cambridge University Press

Once the modeling of the different forces is established, the global force vector in $\mathfrak{R}_m(O, x_m, y_m, z_m)$ can be expressed as

$$f^m = \begin{bmatrix} \mathcal{U}_x \\ \mathcal{U}_y \\ \mathcal{T} \end{bmatrix} + \mathrm{R}^T \begin{bmatrix} \mathcal{D}x \\ \mathcal{D}y \\ \mathcal{D}z \end{bmatrix} + \mathrm{R}^T \begin{bmatrix} 0 \\ 0 \\ \mathcal{G} \end{bmatrix}$$
$$= \begin{bmatrix} -\sum_{i=1}^{4} \mathcal{U}_{xi} \\ -\sum_{i=1}^{4} \mathcal{U}_{yi} \\ \sum_{i=1}^{4} f_i \end{bmatrix} + \mathrm{R}^T \begin{bmatrix} -\mathcal{K}_{\mathcal{D}x}\dot{x} \\ -\mathcal{K}_{\mathcal{D}y}\dot{y} \\ -\mathcal{K}_{\mathcal{D}z}\dot{z} \end{bmatrix} + \mathrm{R}^T \begin{bmatrix} 0 \\ 0 \\ -\mathrm{mg} \end{bmatrix} \quad \ldots(18)$$

where $\mathrm{R}^{-1} = \mathrm{R}^T$.

3.2.2 Moments

Herein, we seek to present the different moments around the three axes x_m, y_m and z_m. The quadrotor can turn about these axes by applying the moments τ_φ, τ_θ and τ_ψ, respectively. The moments of roll and pitch (τ_φ,τ_θ) are induced by the thrust forces f_i generated by each rotor. In our case, they depend on the folding angle of the arms as

$$\tau_{(\varphi,\theta)} = \sum_{i=1}^{4} \overrightarrow{\mathbb{G}\mathbb{G}}_{(3,i)} \times \overrightarrow{f_i}$$
$$= \begin{bmatrix} \sum_{i=1}^{4} (y_{3,i}(t) - y_G(t)) f_i \\ -\sum_{i=1}^{4} (x_{3,i}(t) - x_G(t)) f_i \end{bmatrix} \quad \ldots(19)$$

The moving coordinates of the centre of gravity of the rotors are given as

$$\begin{cases} x_{3,1}(t) = \frac{a}{2} + (L_2 + r_3)\sin\psi_1(t) \\ x_{3,2}(t) = \frac{a}{2} + (L_2 + r_3)\cos\psi_2(t) \\ x_{3,3}(t) = -\frac{a}{2} - (L_2 + r_3)\sin\psi_3(t) \\ x_{3,4}(t) = -\frac{a}{2} - (L_2 + r_3)\cos\psi_4(t) \\ y_{3,1}(t) = -\frac{a}{2} - (L_2 + r_3)\cos\psi_1(t) \\ y_{3,2}(t) = \frac{a}{2} + (L_2 + r_3)\sin\psi_2(t) \\ y_{3,3}(t) = \frac{a}{2} + (L_2 + r_3)\cos\psi_3(t) \\ y_{3,4}(t) = -\frac{a}{2} - (L_2 + r_3)\sin\psi_4(t) \end{cases} \quad \ldots(20)$$

In addition, the total yaw moment τ_ψ along z_m-axis is considered to be

$$\tau_\psi = \sum_{i=1}^{4} (-1)^{i+1} \mathcal{Q}_i \quad \ldots(21)$$

where $\mathcal{Q}_i = C_\mathcal{Q} \rho A R_r (\Omega_i R_r)^2$.

https://doi.org/10.1017/aer.2021.54 Published online by Cambridge University Press

Wind effects can generate an aerodynamic friction torque $\mathcal{M}_{\mathcal{A}} \in \mathbb{R}^3$, expressed as

$$\begin{aligned}\mathcal{M}_{\mathcal{A}} &= (\mathcal{M}_{\mathcal{A}x}\ \mathcal{M}_{\mathcal{A}y}\ \mathcal{M}_{\mathcal{A}z})^T \\ &= \text{diag}\left(\mathcal{K}_{\mathcal{A}x}\ \mathcal{K}_{\mathcal{A}y}\ \mathcal{K}_{\mathcal{A}z}\right)\dot{\varsigma}^2\end{aligned} \quad \ldots(22)$$

The flapping moment $\mathcal{L}_i$ is created due to the difference in lift between the blade that moves back and the blade that advances. It is given by its two components as

$$\mathcal{L}_x = \sum_{i=1}^{4}(-1)^{i+1}\mathcal{L}_{xi},\ \mathcal{L}_y = \sum_{i=1}^{4}(-1)^{i+1}\mathcal{L}_{yi} \quad \ldots(23)$$

where $\mathcal{L}_i = C_{\mathcal{L}}AR_r(\Omega_i R_r)^2$.

In the case when the quadrotor rotates around its x_m-axis, a gyroscopic moment $\mathcal{O}_y$ occurs on each rotating rotor along the y_m-axis. However, when the quadrotor rotates around its y_m-axis, the rotating rotors have also a gyroscopic moment $\mathcal{O}_x$ along the x_m-axis. The expression of the global gyroscopic moment is

$$\mathcal{O}_x = \mathfrak{J}_r q\sum_{i=1}^{4}(-1)^{i+1}\Omega_i,\ \mathcal{O}_y = -\mathfrak{J}_r p\sum_{i=1}^{4}(-1)^{i+1}\Omega_i \quad \ldots(24)$$

where $\mathfrak{J}_r$ is the inertia of the rotor.

Another moment is produced from the hub forces along the x_m-axis and y_m-axis, called the hub moment. It is given as

$$\begin{aligned}\mathcal{H} = &\sum_{i=1}^{4}(x_{3,i}(t) - x_G(t))(\mathrm{s}_{\psi_i(t)}\mathcal{U}_{xi} + \mathrm{c}_{\psi_i(t)}\mathcal{U}_{yi}) \\ &- \sum_{i=1}^{4}(y_{3,i}(t) - y_G(t))(\mathrm{c}_{\psi_i(t)}\mathcal{U}_{xi} - \mathrm{s}_{\psi_i(t)}\mathcal{U}_{yi})\end{aligned} \quad \ldots(25)$$

Finally, the global moment vector τ^m, which includes various moments, is expressed as

$$\begin{aligned}\tau^m &= \begin{bmatrix}\tau_\varphi + \mathcal{O}_x + \mathcal{L}_x + \mathcal{M}_{\mathcal{A}x} \\ \tau_\theta + \mathcal{O}_y + \mathcal{L}_y + \mathcal{M}_{\mathcal{A}y} \\ \tau_\psi + \mathcal{H} + \mathcal{M}_{\mathcal{A}z}\end{bmatrix} \\ &= \begin{bmatrix}\sum_{i=1}^{4}[(y_{3,i}(t) - y_G(t))f_i + \mathfrak{J}_r q(-1)^{i+1}\Omega_i + (-1)^{i+1}\mathcal{L}_{xi}] + \mathcal{K}_{\mathcal{A}x}p^2 \\ \sum_{i=1}^{4}[(x_G(t) - x_{3,i}(t))f_i - \mathfrak{J}_r p(-1)^{i+1}\Omega_i + (-1)^{i+1}\mathcal{L}_{yi}] + \mathcal{K}_{\mathcal{A}y}q^2 \\ \sum_{i=1}^{4}[(-1)^{i+1}Q_i + (x_{3,i}(t) - x_G(t))(\mathrm{s}_{\psi_i(t)}\mathcal{U}_{xi} + \mathrm{c}_{\psi_i(t)}\mathcal{U}_{yi}) \\ -(y_{3,i}(t) - y_G(t))(\mathrm{c}_{\psi_i(t)}\mathcal{U}_{xi} - \mathrm{s}_{\psi_i(t)}\mathcal{U}_{yi})] + \mathcal{K}_{\mathcal{A}z}r^2\end{bmatrix}\end{aligned} \quad \ldots(26)$$

Equation (26) clearly shows the major difference in the dynamic model with respect to the conventional quadrotor.

https://doi.org/10.1017/aer.2021.54 Published online by Cambridge University Press

3.3 Servomotor modeling

The proposed dynamic model for the servomotors is based on the physical principles for modern Dynamixel servomotors[65] and includes several phenomena such as viscous friction and saturation. These servomotors are used to rotate the arms of the proposed quadrotor. They are controlled by an internal Proportional–Integral–Derivative (PID) regulator. After some mathematical operations and using the Laplace transformation, the mechanical open-loop transfer function as well as the electrical part are given respectively by the following relations:

$$\frac{\theta_l(s)}{\mathcal{I}(s)} = \frac{NnK_t}{(J_l + J_m N^2 n)s^2 + (b_m N^2 n)s} \quad \ldots(27)$$

$$\mathcal{I}(s) = \frac{U(s)}{R_\mathcal{I} + L_\mathcal{I} s} - \frac{sN\theta_l(s)}{k_w(R_\mathcal{I} + L_\mathcal{I} s)} \quad \ldots(28)$$

The closed-loop transfer function including the PID regulator is given as follows:

$$\mathcal{F}(s) = \frac{A_\mathcal{F}(k_D s^2 + k_P s + k_I)}{B_\mathcal{F} s^3 + C_\mathcal{F} s^2 + D_\mathcal{F} s + E_\mathcal{F}} \quad \ldots(29)$$

The servomotor parameters are described in Table 6, where $A_\mathcal{F}$, $B_\mathcal{F}$, $C_\mathcal{F}$, $D_\mathcal{F}$, $E_\mathcal{F}$ are constants specific to the servomotor.

Table 6
Dynamixel actuator and rotor parameters[65,66]

Parameter	Description	Value
θ_l	Rotation angle	–
$\mathcal{I}, I$	Input currents	–
$U, \mathcal{V}$	Input voltages	–
N	Gear ratio	193
n	Gear efficiency	0.836
K_t	Torque constant	0.0107Nm/A
k_r	Load torque constance	3.452×10^{-7}Nm/A
J_l	Load inertia moment	Variable
J_m	Dynamixel inertia	8.68×10^{-8}kg m^2
$\mathfrak{J}_r$	Rotor inertia	2.83×10^{-5}Nm/rad/s^2
b_m	Friction	8.87×10^{-8}Nms
K_w	Speed constant	93.1rad/V
R_I	Internal resistance	8.3Ω
R_r	Internal resistance	–
L_I	Inductance of Dynamixel	2.03×10^{-3}H
L	Inductance of motor	–
k_e	Electric torque constant	–
k_m	Mechanic torque constant	–
C_s	Friction constant	5.36×10^{-3}
q_1	Constant	6.0612
q_3	Constant	280.19

https://doi.org/10.1017/aer.2021.54 Published online by Cambridge University Press

3.4 Rotor modeling

Knowledge of the rotor dynamics allows low-level rotor control. This control presents the energy required by the different rotors in terms of the current and voltage needed to turn them with a desired speed. Studies on brushless motors have shown that rotors are driven by Direct-Current (DC) motors, they can be modeled as[66]

$$\begin{cases} \mathcal{V} = R_r I + L\dfrac{dI}{dt} + E \\ \mathcal{T}_m = \mathfrak{J}_r \dfrac{d\Omega}{dt} + C_s + \mathcal{T}_r \end{cases} \quad \ldots(30)$$

Since this type of motors usually have a negligible inductance, the rotor dynamics can be approximated as

$$\mathcal{V} = \frac{\dot{\Omega} + q_2\Omega^2 + q_1\Omega + q_0}{q_3} \quad \ldots(31)$$

where $E = k_e\Omega$, $\mathcal{T}_m = k_m I$, $\mathcal{T}_r = k_r\Omega^2$, $q_0 = \dfrac{C_s}{\mathfrak{J}_r}$, $q_1 = \dfrac{k_e k_m}{R_r\mathfrak{J}_r}$, $q_2 = \dfrac{k_r}{\mathfrak{J}_r}$ and $q_3 = \dfrac{k_m}{R_r\mathfrak{J}_r}$.

3.5 Control allocation matrix

We assume that the quadrotor is controlled to follow paths with small speed and maneuvers. Consequently, the Euler angular velocities are considered as $\dot{\varphi} \approx p$, $\dot{\theta} \approx q$, $\dot{\psi} \approx r$ and the aerodynamic coefficients are taken with their simplified formulas[67] as follows:

$$f_i = b\Omega_i^2,\ \mathcal{Q}_i = d\Omega_i^2 \quad \ldots(32)$$

where b and d are the thrust and drag coefficients, respectively.

The transformable quadrotor has eight control inputs. The control vector of its altitude and attitude is defined as $u = (u_1, u_2, u_3, u_4)^T \in \mathbb{R}^4$, while the control vector of the servomotor positions is given as $s = (u_5, u_6, u_7, u_8)^T \in \mathbb{R}^4$, where

$$u_1 = \mathcal{T},\ \ u_2 = \tau_\varphi,\ \ u_3 = \tau_\theta,\ \ u_4 = \tau_\psi \quad \ldots(33)$$

The relation between the total thrust force, the moments applied to the CoG and the propeller square velocities can be expressed in matrix notation as

$$u = \Delta(\psi_i(t))\eta \quad \ldots(34)$$

with $\eta \in \mathbb{R}^4$ is the vector including the squared propeller velocities:

$$\eta = \left[\Omega_1^2, ..., \Omega_4^2\right]^T \quad \ldots(35)$$

and $\Delta(\psi_i(t)) \in \mathbb{R}^{4*4}$ is the control allocation matrix. The latter represents a crucial element in the architecture of the quadrotor control as it transforms the square of the rotational speeds of the propellers $\Omega_i^2|_{i=1,...,4}$ into a total thrust force $\mathcal{T}$ and moments τ_φ, τ_θ, τ_ψ as

$$\begin{bmatrix} u_1 \\ u_2 \\ u_3 \\ u_4 \end{bmatrix} = \Delta(\psi_i(t)) \begin{bmatrix} \Omega_1^2 \\ \Omega_2^2 \\ \Omega_3^2 \\ \Omega_4^2 \end{bmatrix} \quad \ldots(36)$$

https://doi.org/10.1017/aer.2021.54 Published online by Cambridge University Press

Considering the new expressions of $(\mathcal{T}, \tau_\varphi, \tau_\theta, \tau_\psi)$ generated by the quadrotor, given by (19) and (32), the dynamic allocation matrix $\Delta(\psi_i(t))$ becomes

$$\Delta(\psi_i(t)) = \begin{bmatrix} b & b\left[y_{3,1}(t) - y_G(t)\right] & b\left[x_G(t) - x_{3,1}(t)\right] & d \\ b & b\left[y_{3,2}(t) - y_G(t)\right] & b\left[x_G(t) - x_{3,2}(t)\right] & -d \\ b & b\left[y_{3,3}(t) - y_G(t)\right] & b\left[x_G(t) - x_{3,3}(t)\right] & d \\ b & b\left[y_{3,4}(t) - y_G(t)\right] & b\left[x_G(t) - x_{3,4}(t)\right] & -d \end{bmatrix}^T \quad \ldots (37)$$

The elements of the matrix $\Delta(\psi_i(t))$ depend strongly on the geometrical variations. Therefore, they must be instantly updated to be taken into account when the configuration changes.

Remark 2: The four servomotors used to rotate the quadrotor arms are controlled separately to achieve the desired aerial configuration, and the control allocation matrix presented in this section does not contain any mapping to these servomotors.

To establish the complete dynamic model, translational velocities and accelerations are expressed in the frame $\mathfrak{R}_i(o_i, x_i, y_i, z_i)$. However, the angular velocities and accelerations are expressed in the frame $\mathfrak{R}_m(O, x_m, y_m, z_m)$.

Based on Equations (15), (18) and (26), the simplified control model can be arranged as (40).

The choice of the state vector is

$$X = \left[\varphi, \dot{\varphi}, \theta, \dot{\theta}, \psi, \dot{\psi}, z, \dot{z}, x, \dot{x}, y, \dot{y}\right]^T \quad \ldots (38)$$

such as

$$X = \left[x_1, x_2, x_3, x_4, x_5, x_6, x_7, x_8, x_9, x_{10}, x_{11}, x_{12}\right]^T \quad \ldots (39)$$

$$\begin{cases} \dot{x}_1 = x_2 \\ \dot{x}_2 = \beta_1(t)x_4x_6 + \beta_2(t)x_4\Omega_r + \beta_3(t)u_2 + \beta_4(t){x_2}^2 \\ \dot{x}_3 = x_4 \\ \dot{x}_4 = \beta_5(t)x_2x_6 + \beta_6(t)x_2\Omega_r + \beta_7(t)u_3 + \beta_8(t){x_4}^2 \\ \dot{x}_5 = x_6 \\ \dot{x}_6 = \beta_9(t)x_2x_4 + \beta_{10}(t)u_4 + \beta_{11}(t){x_6}^2 \\ \dot{x}_7 = x_8 \\ \dot{x}_8 = -g + u_1\dfrac{cos(x_1)cos(x_3)}{m} + \beta_{12}x_8 \\ \dot{x}_9 = x_{10} \\ \dot{x}_{10} = u_1\frac{u_x}{m} + \beta_{13}x_{10} \\ \dot{x}_{11} = x_{12} \\ \dot{x}_{12} = u_1\frac{u_y}{m} + \beta_{14}x_{12} \end{cases} \quad \ldots (40)$$

https://doi.org/10.1017/aer.2021.54 Published online by Cambridge University Press

where

$$\beta_1(t)=\frac{I_{yy}(\psi_i(t))-I_{zz}(\psi_i(t))}{I_{xx}(\psi_i(t))},\quad \beta_2(t)=\frac{-\mathfrak{J}_r}{I_{xx}(\psi_i(t))}\quad \beta_3(t)=\frac{1}{I_{xx}(\psi_i(t))},$$
$$\beta_5(t)=\frac{I_{zz}(\psi_i(t))-I_{xx}(\psi_i(t))}{I_{yy}(\psi_i(t))}\ \beta_4(t)=\frac{-\mathcal{K}_{\mathcal{A}x}}{I_{xx}(\psi_i(t))},\ \beta_9(t)=\frac{I_{xx}(\psi_i(t))-I_{yy}(\psi_i(t))}{I_{zz}(\psi_i(t))}\ \beta_6(t)=\frac{\mathfrak{J}_r}{I_{yy}(\psi_i(t))},$$
$$\beta_7(t)=\frac{1}{I_{yy}(\psi_i(t))},\ \beta_8(t)=\frac{-\mathcal{K}_{\mathcal{A}y}}{I_{yy}(\psi_i(t))}$$
$$\beta_{10}(t)=\frac{1}{I_{zz}(\psi_i(t))},\ \beta_{11}(t)=\frac{-\mathcal{K}_{\mathcal{A}z}}{I_{zz}(\psi_i(t))},\ \beta_{12}=\frac{-\mathcal{K}_{\mathcal{D}z}}{\mathfrak{m}}$$
$$\beta_{13}=\frac{-\mathcal{K}_{\mathcal{D}x}}{\mathfrak{m}},\ \beta_{14}=\frac{-\mathcal{K}_{\mathcal{D}y}}{\mathfrak{m}},\ \Omega_r=\sum_{i=1}^{4}(-1)^{i+1}\Omega_i^2$$

4.0 CONTROL

In this section, we design and investigate the efficiency of the proposed controller. The controller will be applied on the transformable quadrotor, taking into account the variation of the CoG, the inertia and the allocation matrix. It is designed considering the model presented in equation (40) and applied to the generic model developed in Section 3.

4.1 Control review

According to recent literature, a few strategies have been developed to control UAVs subject with variable geometric properties.

In Ref.[62], the authors discussed the use of Linear Quadratic Regulation (LQR) for a quadrotor with variable geometry arms, where the angles between the arms change but the structure always remains symmetrical. The same controller is adopted in Refs[13,26] to stabilize a morphing quadrotor with rotating and extendable arms. Adaptive LQR was exploited by Ref.[10] to control a foldable quadrotor with the goal of guaranteeing stable flight. Considering the rotation of the quadrotor arms, Xiong et al.[29] were interested in optimizing energy consumption during the flight, where the attitude and trajectory of the prototype were controlled using two PID controllers. An X-Morf quadrotor, with two independent rotating arms, was designed in Ref.[35], where Model Reference Adaptive Control (MRAC) is implemented to deal with the changes of the CoG and the inertia and to control the angular velocities. In addition, a classic PID controller combined with a dynamic reversal process was exploited for attitude control. Riviere et al.[18] used an adaptive PID controller to control a quad-morphing robot, taking into account the variation of the inertia matrix. Zhao et al.[43] developed a controller for a transformable multirotor based on the Linear Quadratic Integral (LQI) for attitude and altitude control. However, position control in the horizontal plane was achieved by a conventional PID. In addition, the developed controller is based on a simplified model and assumes that the CoG is always close to the geometric centre. The authors in Ref.[15] presented an LQR attitude controller for an aerial morphing robot that can fold and unfold its arms vertically. A quadrotor with extendable arms was controlled in position and attitude using a conventional PID regulator in Ref.[50]. The same control strategy was exploited to control the position and attitude of the transformable UAV in Refs.[16,42,53]. Recently, Raj et al. proposed a dynamic feedback linearisation-based strategy in Ref.[68] for attitude control of a transformable quadrotor UAV.

https://doi.org/10.1017/aer.2021.54 Published online by Cambridge University Press

Analyzing the above-cited works, it can be concluded that the most widely used techniques are PID, LQR, LQI and feedback linearisation, or their adaptive versions. Furthermore, due to the complexity of the control strategy, they did not take into account the variation of the CoG, the inertia and the allocation matrix at the same time.

In the current work, we propose the design of a new approach for the control of the designed transformable quadrotor. This approach was chosen for its effectiveness with respect to geometric variations, as well as the limitations of the control strategies proposed in literature. In addition, it is very suitable for the hierarchical architecture of the studied system, and it is also approached as a system control tool with various unknown parameters.

4.2 Architecture and controller design

In this paper, the controller is designed to ensure the tracking of the desired trajectory (x_d, y_d, z_d) along the three axes in addition to the yaw angle, with the different quadrotor morphologies previously given according to the mission. These reference trajectories are provided on-line by a Trajectory Generator Block (TGB), as illustrated in Fig. 6. The quadrotor is controlled by the speeds of the four motors Ω_i, which are deduced from the allocation matrix.

The transformable quadrotor is considered as a series of fixed-configuration quadrotors, where each configuration is defined by a range of angles and each range has its own parameters (gains k_i). Consequently, the adaptation block (Fig. 6) contains the gains for each configuration. When the angles correspond to a configuration, the adaptation block assigns the corresponding parameters to the different controllers to calculate the appropriate control laws.

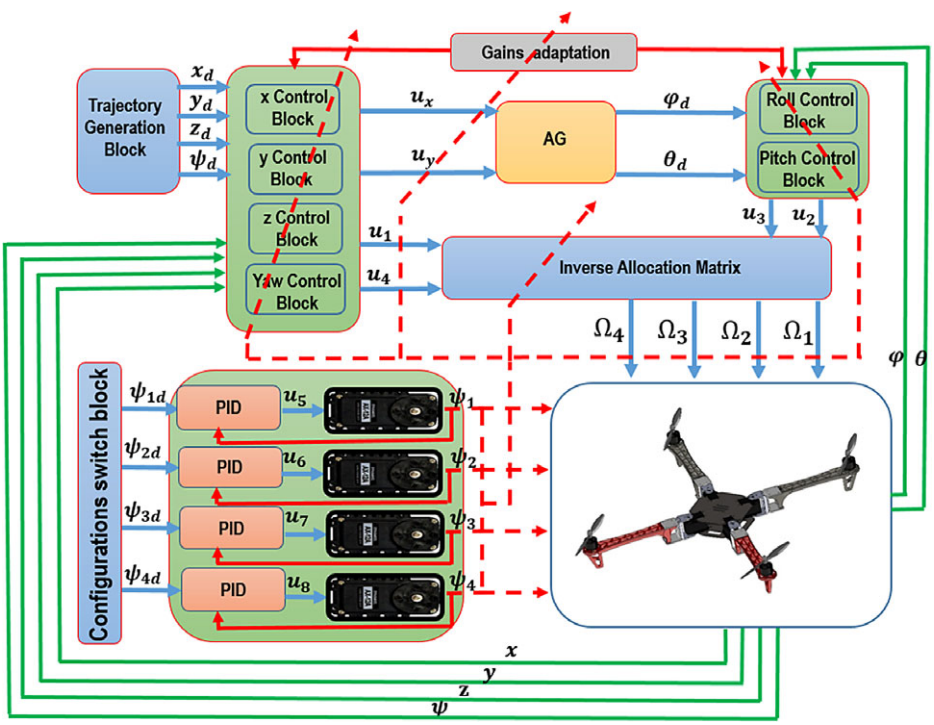

Figure 6. Control architecture of the transformable quadrotor.

https://doi.org/10.1017/aer.2021.54 Published online by Cambridge University Press

The CoG, the inertia and the allocation matrix vary instantaneously and have to be recomputed on-line and incorporated into the generic model of the system when the configuration is changed (Fig. 6).

The angular position of the four servomotors is controller using PID controllers (u_5, u_6, u_7, u_8), as displayed in Fig. 6. Their controllers are given by the following equation:

$$u_j = k_P e_{\psi_i(t)} + k_I \int_0^t e_{\psi_i(t)} dt + k_D \dot{e}_{\psi_i(t)}, j, i = 5, .., 8 \quad \ldots (41)$$

where $e_{\psi_i(t)} = \psi_{id} - \psi_i$ is the tracking error. k_P, k_I and k_D denote the usual proportional, integral and derivative tuning gains. They are positive constants.

The servomotors control the position of the arms. These positions are used in the adaptation block to calculate the gains of the quadrotor controllers and by other blocks to update the current inertia matrix, the allocation matrix as well as the CoG for each configuration (Fig. 6). Then, the inertia terms will also be used by the various controller blocks.

The two controls u_x and u_y and the desired yaw angle ψ_d are used to calculate the roll and pitch angles, which are required to achieve the desired position.

The different control laws will be implemented and tested in simulations in the next section.

4.3 Controller synthesis

The first subsystem is given as

$$\begin{cases} \dot{x}_1 = x_2 \\ \dot{x}_2 = \beta_1(t) x_4 x_6 + \beta_2(t) x_4 \Omega_r + \beta_3(t) U_2 + \beta_4(t) {x_2}^2 \end{cases} \quad \ldots (42)$$

For clarity and conciseness, steps 1 and 2 are described with detailed explanations, while the other steps are simplified.

The detailed design procedure is described in the two following steps.

Firstly:

The tracking error of the first subsystem e_1 and its corresponding derivative $\dot{e_1}$ are expressed as follows:

$$e_1 = x_1 - x_{1d}, \dot{e_1} = x_2 - \dot{x}_{1d} \quad \ldots (43)$$

Let $V_1(e_1)$ be a candidate positive-definite Lyapunov function,

$$V_1(e_1) = \frac{1}{2} {e_1}^2 \quad \ldots (44)$$

The dynamics of $\dot{V}_1(e_1)$ is negative definite as

$$\dot{V}_1(e_1) = -k_1 {e_1}^2, k_1 > 0. \quad \ldots (45)$$

Now, asymptotic Lyapunov stability is guaranteed. For this, the virtual control law of the first subsystem could be chosen as

$$x_{2d} = \dot{x}_{1d} - k_1 e_1. \quad \ldots (46)$$

https://doi.org/10.1017/aer.2021.54 Published online by Cambridge University Press

Secondly:

The tracking error of the second subsystem and its derivative are given as

$$e_2 = x_2 - x_{2d}, \dot{e_2} = \dot{x}_2 - \dot{x}_{2d} \quad \ldots (47)$$

Then, the error dynamics (e_1, e_2) are written as follows:

$$\begin{cases} \dot{e}_1 = e_1 + x_{2d} - \dot{x}_{1d} \\ \dot{e}_2 = \beta_1(t)x_4x_6 + \beta_4(t){x_2}^2 + \beta_2(t)x_4\Omega_r + \beta_3(t)u_2 + k_1(x_2 - \dot{x}_{1d}) - \ddot{x}_{1d} \end{cases} \quad \ldots (48)$$

To obtain the control law u_2, we increase the already existing Lyapunov function (44) by adding a quadratic term.

Consider the new Lyapunov function candidate,

$$V_2(e_1, e_2) = V_1(e_1) + \frac{1}{2}{e_2}^2. \quad \ldots (49)$$

Its derivative is negative definite as

$$\dot{V}_2(e_1, e_2) = -k_1{e_1}^2 - k_2{e_2}^2 < 0, k_2 > 0. \quad \ldots (50)$$

To achieve objective (50) and ensure Lyapunov stability, the control law is designed as

$$u_2 = \frac{1}{\beta_3(t)}[-\beta_1(t)x_4x_6 - \beta_4(t){x_2}^2 - \beta_2(t)x_4\Omega_r + \ddot{x}_{1d} - k_1(-k_1e_1 + e_2) - e_1 - k_2e_2] \quad \ldots (51)$$

To extract the other controllers, we follow the same steps as above.

5.0 SIMULATION

In this section, a MATLAB simulation is developed to validate the generic model developed in Section 3 and then evaluate the efficiency of the proposed controller. Before that, it is very useful to define the different parameters used in the simulation.

To identify the best PID parameters, simulations are performed for different position goals using the closed-loop model of the servomotors, where the parameters k_P, k_I and k_D are tuned manually to achieve a similar response in terms of steady-state error, response time and overshoot compared with the real servomotor response. The corresponding gains are presented in Table 7.

The sets of coefficients for the controller considered in the simulation are defined in Table 8.

Table 7
Servo controller gains

Gain	k_P	k_I	k_D
Value	3.22	1.72	1.52

https://doi.org/10.1017/aer.2021.54 Published online by Cambridge University Press

Table 8
Controller parameters

Parameter	X	H	O	Y	YI	T
k_1	0.25	1.27	4.32	0.94	2.71	0.61
k_2	0.37	0.33	2.35	0.11	4.91	0.14
k_3	4.05	2.41	0.23	5.02	4.65	1.71
k_4	2.77	1.59	1.53	4.73	0.084	0.52
k_5	0.75	0.066	1.25	1.25	1.25	0.088
k_6	0.23	0.28	1.31	2.45	1.53	1.17
k_7	10.11	11.19	10.26	13.47	9.31	8.93
k_8	11.45	9.76	10.57	9.23	11.12	8.81
k_9	1.11	2.11	1.23	1.46	1.47	0.46
k_{10}	2.14	1.17	1.26	1.48	1.44	0.7
k_{11}	1.89	1.91	1.42	1.51	1.51	1.16
k_{12}	2.12	1.47	2.33	4.82	4.64	0.53

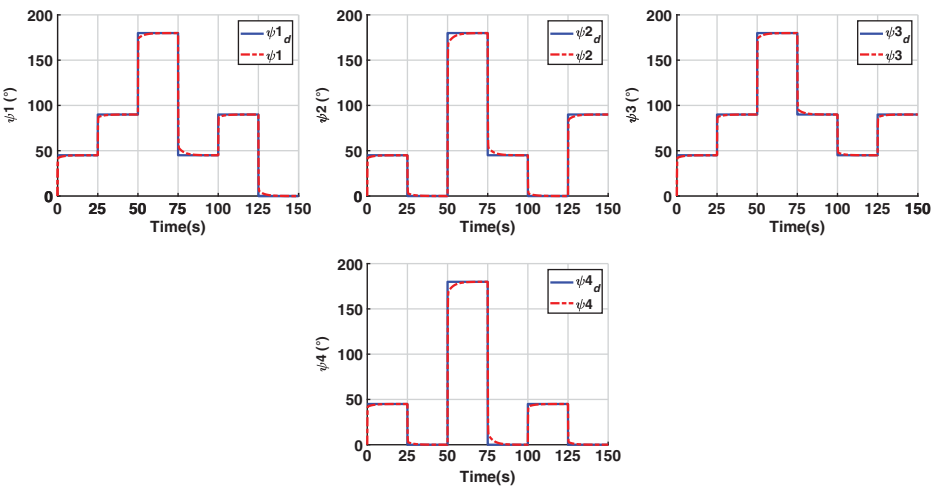

Figure 7. Evolution of servomotor angles.

5.1 Flight scenario

In this scenario, we want to make a circular trajectory followed by the quadrotor where it changes its configuration every 25s. To achieve this, the quadrotor starts in the classic "X" configuration and then changes shape to other special morphologies such as "H", "O", "Y", "YI" and "T" (Fig. 3).

The simulation results are shown in Figs 7, 8, 9, 10, 11, 12 and 13.

5.1.1 Results and discussion for the flight scenario

Figure 7 shows the evolution of the real and desired positions of the servomotors used to rotate the four arms of the quadrotor. It is observed that the outputs of the four servomotors

https://doi.org/10.1017/aer.2021.54 Published online by Cambridge University Press

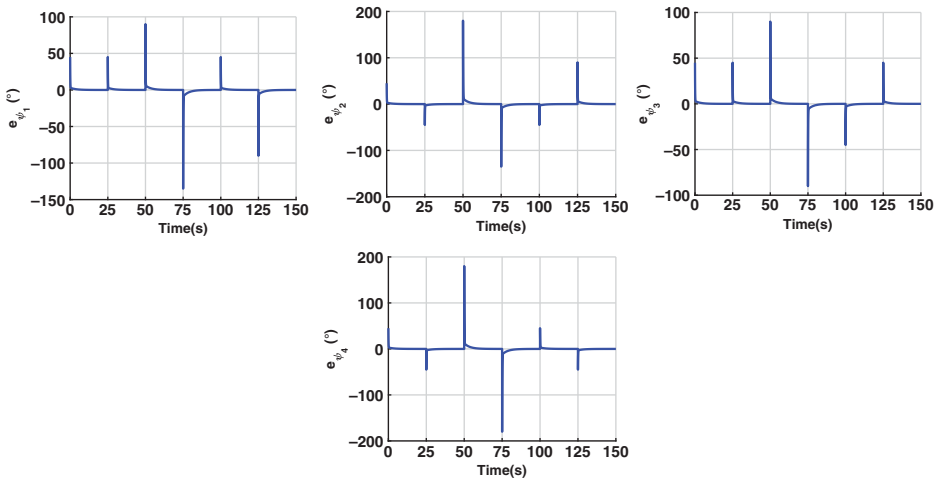

Figure 8. Evolution of servomotor position errors.

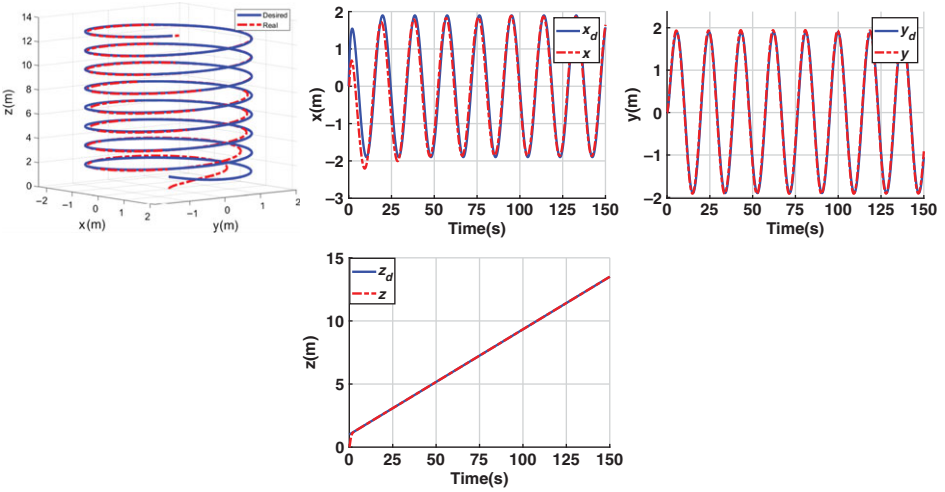

Figure 9. Evolution of 3D trajectory and positions.

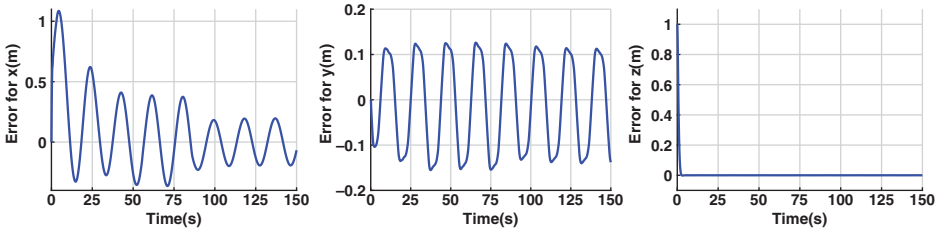

Figure 10. Evolution of position errors.

https://doi.org/10.1017/aer.2021.54 Published online by Cambridge University Press

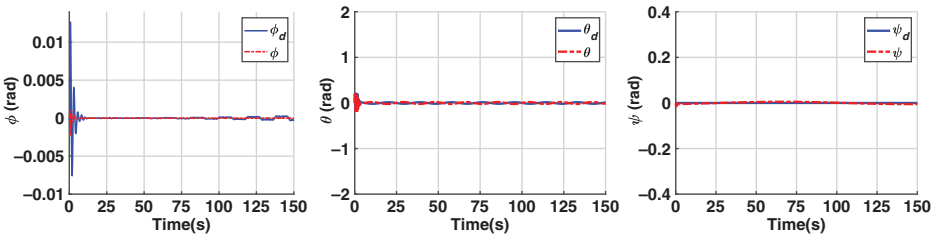

Figure 11. Evolution of Euler angles.

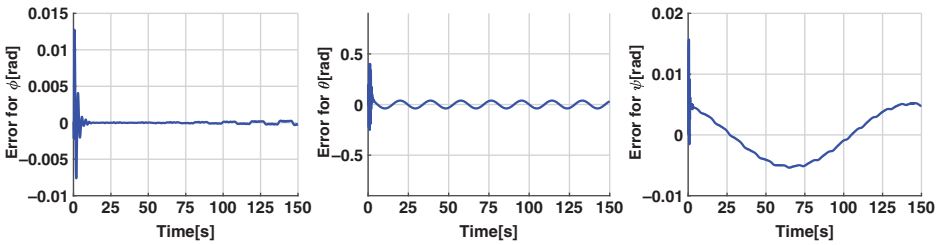

Figure 12. Evolution of attitude errors.

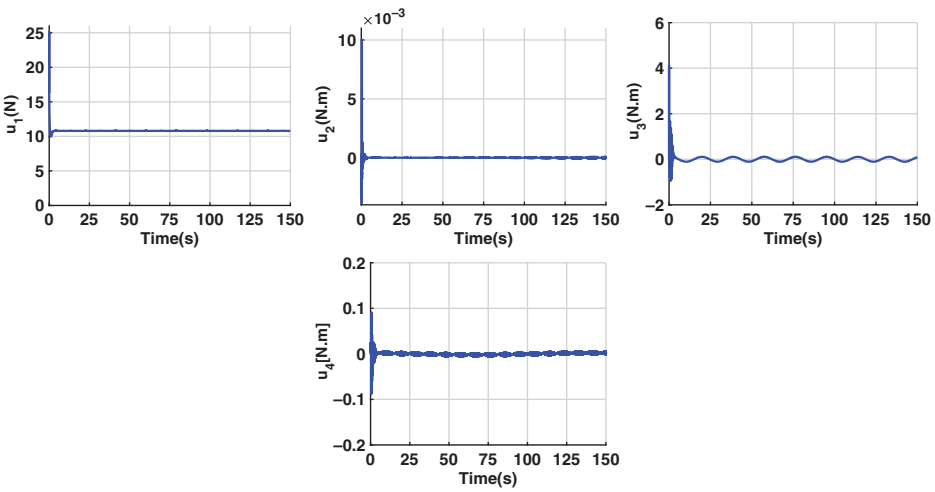

Figure 13. Evolution of control signals.

(ψ_1, ψ_2, ψ_3, ψ_4) achieve their desired positions (ψ_{1d}, ψ_{2d}, ψ_{3d}, ψ_{4d}) at about 3s, without any overshoot. The steady-state errors are approximatively zero. To illustrate this result, the servomotor position errors are plotted in Fig. 8.

The evolution of the 3D trajectory (Fig. 9) shows that the vehicle moves in the horizontal plane (x,y) with a slow variation in altitude. Moreover, the altitude z and the positions (x,y) track their desired trajectories z_d, x_d, y_d.

For the y-axis, the error varies approximately between -0.14 and 0.12m, while for the x-axis, it reaches 1m (approximatively equivalent to 50%) at the beginning of the trajectory

https://doi.org/10.1017/aer.2021.54 Published online by Cambridge University Press

tracking. However, this error decreases rapidly to reach about 0.18m (approximatively equivalent to 9%). The error on the z-axis is equal to 1m at $t = 0$s and then rapidly tends to zero after about 1.8s (Fig. 10).

To reach the desired altitude z_d, the corresponding control increases rapidly at the beginning, and as soon as the rates of variation of the desired and actual altitudes are equal, the control takes a constant value of approximatively 11N (Fig. 13).

From Figs 11 and 12, it is observed that the yaw response follows its desired state, where the tracking error converges towards zero. The yaw dynamics is well illustrated by the evolution of the u_4 control (Fig. 13), increasing at the start and then approaching zero.

For the roll ϕ and pitch θ dynamics, the drone remains stable, with some oscillations appearing in the curves of the angles in Fig. 11. These oscillations produce errors along the two axes (x,y) during the whole flight period, where their values are around zero (Fig. 12).

The evolution of the u_2 and u_3 controls is shown in Fig. 13, where u_2 shows a negligible variation over time while u_3 takes a maximum value of 4.1N at $t = 0s$, then for the rest of the time varies sinusoidally around zero.

In this scenario, we change the configuration of the quadrotor every 25s. The simulation results are satisfactory in terms of tracking, speed and accuracy.

6.0 QUADROTOR PROTOTYPE

The designed prototype is based mainly on the conventional quadrotor structure. This new prototype offers high performance in severe flight conditions, and can consume less energy due to its variable shape. In the case of a loss of efficiency or failure of a rotor, it can be adapted to ensure the continuity of the assigned task by changing its flight configuration to "W" as displayed in Fig. 14. It can tilt its arms around the main body using very powerful servomotors of Dynamixel AX-12A type, which increases the speed of the transformation process in flight compared with the prototypes presented in literature (Figs 3 and 14).

Assumption 3: The realized quadrotor does not make an aggressive rotation of its four arms in flight, and the aerial transformation is carried out in the hovering phase, which prompts us to assume that the aerodynamic phenomena (torques and forces) generated in the transformation phase can be neglected.

Before controlling the quadrotor servomotors, one must first identify the ID of each, because they are placed in series and the ID specifies the destination of the command. Once the identification operation is completed, we connect the Futaba RC reciever to the Arduino board and then identify the RC receiver channel corresponding to each button on an RC transmitter. The latter uses a radio signal in the 2.4GHz band to control the UAV remotely.

Propulsion is assured by four brushless DC motors of type DJI E310, which generate the thrust power. The rotation of these actuaors is controlled by Electronic Speed Controllers (ESCs) of type DJI 420 lite, which operate with a signal frequency of 30–450Hz.

The body angular velocities are represented as p, q and r, being measured physically by three gyroscopic sensors integrated into a Pixhawk flight controller card.

The choice of manufacturing material is a very important step in the mechanical design. However, the central body is based on the structure of the DJI F450 quadrotor, which is constructed using carbon fibre material due to its reliability in terms of lightness, stiffness, high tensile strength, low thermal expansion and greatest compatibility with the other components.

https://doi.org/10.1017/aer.2021.54 Published online by Cambridge University Press

Table 9
Prototype characteristics

Parameters	Value
Total platform weight	1133g
Arm lenght	21cm
Central body length	12cm
Central body width	12cm

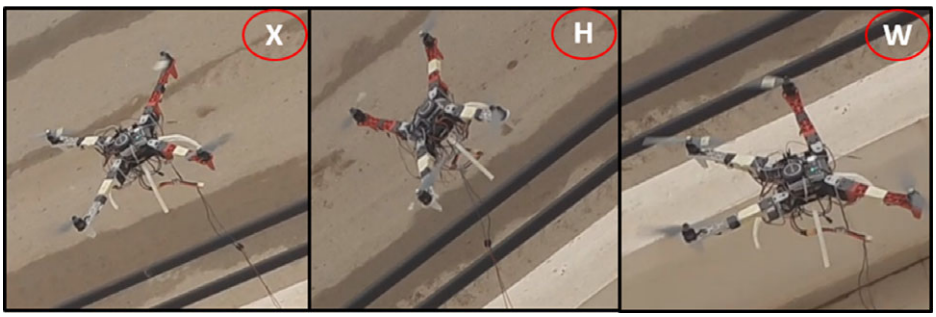

Figure 14. Preliminary flight tests of the transformable quadrotor.

The same material is also used in the actuator joints because of the sensitivity of this part. The rotating arms are designed of plastic material, which is mainly characterised by its lightness.

The main characteristics of the realised quadrotor are presented in Table 9.

Before implementing the controller in the prototype and carrying out real tests, we fixed the quadrotor to a test bench to eliminate eventual structural faults that could cause flight destabilization.

We used Mission Planer, which allows to load a controller into the Pixhawk autopilot. Once the Pixhawk autopilot is connected with Mission Planner, we calibrate the different sensors. Afterwards, we start the stabilisation tests in the test bench by adjusting the PID controller parameters.

Preliminary flight tests as shown in Fig. 14 were carried out using the same controller, where we selected the best parameters for each configuration.

7.0 CONCLUSIONS AND FUTURE WORK

Based on very recent works, we have presented herein a new state-of-the-art drones class called transformable UAVs, as well as the mechanical design of a quadrotor with rotating arms, the geometric description and the study of the variation of the CoG and inertia. In addition, we have developed a detailed generic model, taking into account the aerodynamic effects, the displacement of the CoG and the variation of the inertia matrix and the allocation matrix. Moreover, to validate this model and ensure the stability of the quadrotor, we have proposed a new control strategy based on the change of the flight configuration. Simulations have shown satisfactory results that demonstrate the efficiency of the proposed controller. Finally, we have illustrated the realised prototype with some experimental configurations during test flights.

https://doi.org/10.1017/aer.2021.54 Published online by Cambridge University Press

Future work will include flight tests with all the morphologies in real scenarios and optimization of the consumed energy by seeking the optimal morphology during flight. Also, the stability of each flight configuration against atmospheric turbulence will be evaluated and investigated.

REFERENCES

1. GUPTE, S., MOHANDAS, P.I.T. and CONRAD, J.M. A survey of quadrotor unmanned aerial vehicles, 2012 Proceedings of IEEE Southeastcon, 2012, pp 1–6.
2. PURI, A. A survey of unmanned aerial vehicles (UAV) for traffic surveillance, 2005, pp 1–29, Department of Computer Science and Engineering, University of South Florida.
3. DERAFA, L., OULDALI, A., MADANI, T. and BENALLEGUE, A. Non-linear control algorithm for the four rotors UAV attitude tracking problem, *Aeronaut. J.*, 2011, **115**, (1165), pp 175–185.
4. FLOREANO, D. and Wood, R.J. Science, technology and the future of small autonomous drones, *Nature*, 2015, **521**, (7553), pp 460–466.
5. MINTCHEV, S. and FLOREANO, D. Adaptive morphology: A design principle for multimodal and multifunctional robots, *IEEE Rob. Autom. Mag.*, 2016, **23**, (3), pp 42–54.
6. CABALLERO, A., SUAREZ, A., REAL, F., VEGA, V.M., BEJAR, M., RODRIGUEZCASTANO, A. and OLLERO, A. First experimental results on motion planning for transportation in aerial long-reach manipulators with two arms, 2018 IEEE/RSJ International Conference on Intelligent Robots and Systems (IROS), 2018, pp 8471–8477.
7. YILMAZ, E., ZAKI, H. and UNEL, M. Nonlinear adaptive control of an aerial manipulation system, 2019 18th European Control Conference (ECC), 2019, pp 3916–3921.
8. DERROUAOUI, S.H., BOUZID, Y., GUIATNI, M., DIB, I. and MOUDJARI, N. Design and modeling of unconventional quadrotors, 2020 28th Mediterranean Conference on Control and Automation (*MED*), IEEE, 2020, pp 721–726.
9. ZHAO, M., KAWASAKI, K., OKADA, K. and INABA, M. Transformable multirotor with two-dimensional multilinks: modeling, control, and motion planning for aerial transformation, *Adv. Rob.*, 2016, **30**, (13), pp 825–845.
10. FALANGA, D., KLEBER, K., MINTCHEV, S., FLOREANO, D. and SCARAMUZZA, D. The foldable drone: A morphing quadrotor that can squeeze and fly, *IEEE Rob. Autom. Lett.*, 2018, **4**, (2), pp 209–216.
11. DERROUAOUI, S.H., BOUZID, Y., GUIATNI, M., HALFAOUI, K., DIB, I. and MOUDJARI, N. Backstepping controller applied to a foldable quadrotor for 3D trajectory tracking, Proceedings of the 17th International Conference on Informatics in Control, Automation and Robotics, 2020, pp 537–544.
12. MINTCHEV, S., SHINTAKE, J. and FLOREANO, D. Bioinspired dual-stiffness origami, *Sci. Rob.*, 2018, **3**, (20).
13. WALLACE, D.A., Dynamics and Control of a Quadrotor with Active Geometric Morphing, PhD Dissertation, University of Washington, 2016.
14. KORNATOWSKI, P.M., FEROSKHAN, M., STEWART, W.J. and FLOREANO, D. A morphing cargo drone for safe flight in proximity of humans, *IEEE Rob. Autom. Lett.*, 2020, **5**, (3), pp 4233–4240.
15. BUCKI, N. and MUELLER, M.W. Design and control of a passively morphing quadcopter, 2019 International Conference on Robotics and Automation (ICRA), 2019, pp 9116–9122.
16. SAKAGUCHI, A., TAKIMOTO, T. and USHIO, T. A novel quadcopter with a tilting frame using parallel link mechanism, 2019 International Conference on Unmanned Aircraft Systems (ICUAS), 2019, pp 674–683.
17. ZHAO, N., LUO, Y., DENG, H. and SHEN, Y. The deformable quadrotor: design, kinematics and dynamics characterization, and flight performance validation, 2017 IEEE/RSJ International Conference on Intelligent Robots and Systems (IROS), 2017, pp 2391–2396.
18. RIVIERE, V., MANECY, A. and VIOLLET, S. Agile robotic fliers: A morphing-based approach, *Soft Rob.*, 2018, **5**, (5), pp 541–553.
19. ZHAO, M., ANZAI, T., SHI, F., CHEN, X., OKADA, K. and Inaba, M. Design, modeling, and control of an aerial robot dragon: A dual-rotorembedded multilink robot with the ability of multi-degree-of-freedom aerial transformation, *IEEE Rob. Autom. Lett.*, 2018, **3**, (2), pp 1176–1183.
20. FABRIS, A., KLEBER, K., FALANGA, D. and SCARAMUZZA, D. Geometry aware compensation scheme for morphing drones, arXiv preprint arXiv:2003.03929, 2020.

https://doi.org/10.1017/aer.2021.54 Published online by Cambridge University Press

21. INVERNIZZI, D., GIURATO, M., GATTAZZO, P. and LOVERA, M. Comparison of control methods for trajectory tracking in fully actuated unmanned aerial vehicles, *IEEE Trans. Control Syst. Technol.*, 2021, **29**, (3), pp 1147–1160. doi: 10.1109/TCST.2020.2992389.
22. ROHR, D., STASTNY, T., VERLING, S. and SIEGWART, R. Attitude and cruise control of a vtol tiltwing uav, *IEEE Rob. Autom. Lett.*, 2019, **4**, (3), pp 2683–2690.
23. LI, G., GABRICH, B., SALDANA, D., DAS, J., KUMAR, V. and YIM, M. Modquad-vi: A vision-based self-assembling modular quadrotor, 2019 International Conference on Robotics and Automation (ICRA), 2019, pp 346–352.
24. DERROUAOUI, S.H., BOUZID, Y., GUIATNI, M. and DIB, I. A comprehensive review on reconfigurable drones: Classification, characteristics, design and control technologies, *Unmanned Syst.*, 2021, **9**, (3), pp 1–27.
25. BAI, Y. and GURURAJAN, S. Evaluation of a baseline controller for autonomous "figure-8" flights of a morphing geometry quadcopter: Flight performance, *Drones*, 2019, **3**, (3), p 70.
26. AVANT, T., LEE, U., KATONA, B. and MORGANSEN, K. Dynamics, hover configurations, and rotor failure restabilization of a morphing quadrotor, 2018 Annual American Control Conference (ACC), 2018, pp 855–4862.
27. DILAVEROGLU, L. and ÖZCAN, O., Minicore: A miniature, foldable, collision resilient quadcopter, 2020 3rd IEEE International Conference on Soft Robotics (RoboSoft), 2020, pp 176–181.
28. TUNA, T., OVUR, S.E., GOKBEL, E. and KUMBASAR, T. Folly: A self foldable and self deployable autonomous quadcopter, 2018 6th International Conference on Control Engineering and Information Technology (CEIT), 2018, pp 1–6.
29. XIONG, H., HU, J. and DIAO, X. Optimize energy efficiency of quadrotors via arm rotation, *J. Dyn. Syst. Meas. Control*, 2019, **141**, (9).
30. FASEL, U., KEIDEL, D., BAUMANN, L., CAVOLINA, G., EICHENHOFER, M. and ERMANNI, P. Composite additive manufacturing of morphing aerospace structures, *Manuf. Lett.*, 2020, **23**, pp 85–88.
31. JIMENEZ-CAN, A., MARTIN, J., HEREDIA, G., OLLERO, A. and CANO, R. Control of an aerial robot with multi-link arm for assembly tasks, 2013 IEEE International Conference on Robotics and Automation, 2013, pp 4916–4921.
32. SUAREZ, A., REAL, F., VEGA, V.M., HEREDIA, G., RODRIGUEZ-CASTAÑO, A. and OLLERO, A. Compliant bimanual aerial manipulation: Standard and long reach configurations, *IEEE Access*, 2020, **8**, pp 88844–88865. doi: 10.1109/ACCESS.2020.2993101.
33. DERROUAOUI, S.H., GUIATNI, M., BOUZID, Y., DIB, I. and MOUDJARI, N. Dynamic modeling of a transformable quadrotor, 2020 International Conference on Unmanned Aircraft Systems (ICUAS), 2020, pp 1714–1719.
34. MINTCHEV, S., DALER, L., L'EPLATTENIER, G., SAINT-RAYMON, L. and FLOREANO, D. Foldable and self-deployable pocket sized quadrotor, 2015 IEEE International Conference on Robotics and Automation (ICRA), 2015, pp 2190–2195.
35. DESBIEZ, A., EXPERT, F., BOYRON, M., DIPERI, J., VIOLLET, S. and RUFFIER, F. X-morf: A crash-separable quadrotor that morfs its x-geometry in flight, 2017 Workshop on Research, Education and Development of Unmanned Aerial Systems (RED-UAS), 2017, pp 222–227.
36. ABDULRAHIM, M. and LIND, R. Flight testing and response characteristics of a variable gull-wing morphing aircraft, AIAA Guidance, Navigation, and Control Conference and Exhibit, 2004, p 5113.
37. BARBARINO, S., BILGEN, O., AJAJ, R.M., FRISWELL, M.I. and INMAN, D.J. A review of morphing aircraft, *J. Intell. Material Syst. Struct.*, 2011, **22**, (9), pp 823–877.
38. MATLOFF, L.Y., CHANG, E., FEO, T.J., JEFFRIES, L., STOWERS, A.K., THOMSON, C. and LENTINK, D. How flight feathers stick together to form a continuous morphing wing, *Science*, 2020, **367**, (6475), pp 293–297.
39. MA, H., SONG, B., PEI, Y. and CHEN, Z. Efficiency change of control surface of a biomimetic wing morphing UAV, *IEEE Access*, 2020, **8**, pp 45 627–45 640.
40. DALER, L.S. Mintchev, C. Stefanini and D. Floreano. A bioinspired multi-modal flying and walking robot, *Bioinspiration Biomimetics*, 2015, **10**, (1), p 016005.
41. MORTON, S. and PAPANIKOLOPOULOS, N. A small hybrid ground-air vehicle concept, 2017 IEEE/RSJ International Conference on Intelligent Robots and Systems (IROS), 2017, pp 5149–5154.
42. D'SA, R., Design of a Transformable Unmanned Aerial Vehicle, PhD Dissertation, University of Minnesota, 2020.

https://doi.org/10.1017/aer.2021.54 Published online by Cambridge University Press

43. ZHAO, M., KAWASAKI, K., CHEN, X., NODA, S., OKADA, K. and INABA, M. Whole-body aerial manipulation by transformable multirotor with two-dimensional multilinks, 2017 IEEE International Conference on Robotics and Automation (ICRA), 2017, pp 5175–5182.
44. BHAT, P., KUFFNER, J., GOLDSTEIN, S. and SRINIVASA, S. Hierarchical motion planning for self-reconfigurable modular robots, 2006 IEEE/RSJ International Conference on Intelligent Robots and Systems, 2006, pp 886–891.
45. HAN, J., HUI, Z., TIAN, F. and CHEN, G. Review on bio-inspired flight systems and bionic aerodynamics, Chin. J. Aeronaut., 2020. https://www.sciencedirect.com/science/article/pii/S1000936120302466?via%3Dihub.
46. JONES, K., BRADSHAW, C., PAPADOPOULOS, J. and PLATZER, M. Bio-inspired design of flapping-wing micro air vehicles, *Aeronaut. J.*, 2005, **109**, (1098), pp 385–393.
47. ZHANG, S., WANG, Z., WU, Y. and YU, Y. Flight dynamic coupling analysis of a bio-inspired elastic-wing aircraft, *Aeronaut. J.*, 2018, **122**, (1250), p 572.
48. SANKET, N.J., SINGH, C.D., GANGULY, K., Fermã¼ller, C. and Aloimonos, Y. Gapflyt: Active vision based minimalist structure-less gap detection for quadrotor flight, *IEEE Rob. Autom. Lett.*, 2018, **3**, (4), pp 2799–2806.
49. FULLER, S.B. Four wings: An insect-sized aerial robot with steering ability and payload capacity for autonomy, *IEEE Rob. Autom. Lett.*, 2019, **4**, (2), pp 570–577.
50. KAMIL, Y., HAZRY, D., WAN, K., RAZLAN, Z.M. and ABU BAK, S. Design a new model of unmanned aerial vehicle quadrotor using the variation in the length of the arm, 2017 International Conference on Artificial Life and Robotics (ICAROB), 2017, pp 723–726.
51. BORST, H.V. Review of v/stol aircraft with tilt-propellers and tiltrotors, *Aeronaut. J.*, 1968, **72**, (693), pp 817–830.
52. GIBERTINI, S.G., AUTERI, F., CAMPANARDI, G., MACCHI, C., ZANOTTI, A. and STABELLINI, A. Wind-tunnel tests of a tilt-rotor aircraft, *Aeronaut. J.*, 2011, **115**, (1167), pp 315.
53. KUMAR, R., SRIDHAR, S., CAZAURANG, F., COHEN, K. and KUMAR, M. Reconfigurable fault-tolerant tilt-rotor quadcopter system, ASME 2018 Dynamic Systems and Control Conference. American Society of Mechanical Engineers Digital Collection, 2018.
54. PARK, S., HER, J., KIM, J. and LEE, D. Design, modeling and control of omni-directional aerial robot, 2016 IEEE/RSJ International Conference on Intelligent Robots and Systems (IROS), 2016, pp 1570–1575.
55. JOSHI, A., TRIPATHI, A. and PONNALGU, R. Modelling and design of a hybrid aerial vehicle combining vtol capabilities with fixed wing aircraft, 2019 6th International Conference on Instrumentation, Control, and Automation (ICA), 2019, pp 47–51.
56. ANGLADE, A., KAI, J.M., HAMEL, T. and SAMSON, C. Automatic control of convertible fixed-wing drones with vectorized thrust, 2019 IEEE 58th Conference on Decision and Control (CDC), 2019, pp 5880–5887.
57. HINTZ, C., TORNO, C. and CARRILLO, L.R.G. Design and dynamic modeling of a rotary wing aircraft with morphing capabilities, 2014 International Conference on Unmanned Aircraft Systems (ICUAS), 2014, pp 492–498.
58. BAI, Y. Control and Simulation of Morphing Quadcopter, PhD Dissertation, Saint Louis University, 2017.
59. LEE, J. Optimization of a modular drone delivery system, 2017 Annual IEEE International Systems Conference (SysCon), 2017, pp 1–8.
60. DA SILVA FERR, M.A., LOPES, G.C., COLOMBINI, E.L. and DA SILVA SI, A. A novel architecture for multipurpose reconfigurable unmanned aerial vehicle (UAV): Concept, design and prototype manufacturing, 2018 Latin American Robotic Symposium, 2018 Brazilian Symposium on Robotics (SBR) and 2018 Workshop on Robotics in Education (WRE), 2018, pp 443–450.
61. MU, B. and CHIRARATTANANON, P. Universal flying objects: Modular multirotor system for flight of rigid objects, *IEEE Trans. Rob.*, 2020, **36**, (2), pp 458–471. doi: 10.1109/TRO.2019.2954679.
62. BARBARACI, G. Modeling and control of a quadrotor with variable geometry arms, *J. Unmanned Veh. Syst.*, 2015, **3**, (2), pp 35–57.
63. SPONG, M.W., HUTCHINSON, S. and VIDYASAGAR, M. *Robot Modeling and Control*, Wiley, New York, 2005. doi: 10.1108/ir.2006.33.5.403.1.
64. BOUZID, Y., SIGUERDIDJANE, H. and BESTAOUI, Y. Generic dynamic modeling for multirotor vtol uavs and robust sliding mode based model free control for 3d navigation, 2018 International Conference on Unmanned Aircraft Systems (ICUAS), 2018, pp 970–979.

https://doi.org/10.1017/aer.2021.54 Published online by Cambridge University Press

65. MAXIMO, M., RIBEIRO, C.H. and AFONSO, R.J. Modeling of a position servo used in robotics applications, Proceedings of the 2017 Simposio Brasileiro de Automaçao Inteligente (SBAI), 2017.
66. DERAFA, L., MADANI, T. and BENALLEGUE, A. Dynamic modeling and experimental identification of four rotors helicopter parameters, 2006 IEEE International Conference on Industrial Technology, 2006, pp 1834–1839.
67. BANGURA, M. and MAHONY, R. Nonlinear dynamic modeling for high performance control of a quadrotor, Proceedings Australasian Conference on Robotics and Automation 2012, 2012.
68. RAJ, N., BANAVAR, R., Abhishek and KOTHARI, M. Attitude control of novel tail sitter: Swiveling biplane–quadrotor, *J. Guidance Control Dyn.*, 2020, **43**, (3), pp 599–607.

Saddam Hocine Derrouaoui received his engineering degree from the Ecole Supérieure Ali Chabati, Réghaia, Algiers, Algeria (in 2016) and his master's degree in systems guidance and automatic from the same school (in 2016). He is now pursuing a doctor's degree in automation in the Laboratory of Complex Systems Control and Simulators (CSCS) of the Ecole Militaire Polytechnique (EMP), Bordj-el-Bahri, Algiers, Algeria. His research interests include nonlinear control, unmanned aerial vehicles, transformable and reconfigurable drones, mobile robots and manipulator arms.

Yasser Bouzid received his engineering degree from the Ecole Militaire Polytechnique (EMP), Bordj-el-Bahri, Algiers, Algeria (in 2013) and his master of science (MSc) from the University of Paris XI, France (in 2015). He received his Ph.D. degree in automation from Paris Saclay University in 2018. He is currently an assistant professor at the EMP and a member of the Laboratory of Complex Systems Control and Simulators (CSCS). His research interests include nonlinear control, fault-tolerant control, observation and estimation, path planning, heuristic algorithms, unmanned aerial vehicles, mobile robots, multi-agent systems and soft robotics.

Mohamed Guiatni received his bachelor of engineering and master of science (MSc) degrees from the Ecole Militaire Polytechnique (EMP), Bordj-el-Bahri, Algiers, Algeria and his PhD degree from the University of Evry, France in 2009. He is currently the head of the Complex Systems Control and Simulators Laboratory and full professor at the EMP. His research interests include haptic devices design and control, mechatronics, rehabilitation robotics, interactive simulation for military and medical applications, and UAV design and control.

https://doi.org/10.1017/aer.2021.54 Published online by Cambridge University Press